

UniFormer: Unifying Convolution and Self-attention for Visual Recognition

Kunchang Li, Yali Wang, Junhao Zhang, Peng Gao, Guanglu Song,
Yu Liu, Hongsheng Li and Yu Qiao

Abstract—It is a challenging task to learn discriminative representation from images and videos, due to large local redundancy and complex global dependency in these visual data. Convolution neural networks (CNNs) and vision transformers (ViTs) have been two dominant frameworks in the past few years. Though CNNs can efficiently decrease local redundancy by convolution within a small neighborhood, the limited receptive field makes it hard to capture global dependency. Alternatively, ViTs can effectively capture long-range dependency via self-attention, while blind similarity comparisons among all the tokens lead to high redundancy. To resolve these problems, we propose a novel Unified transFormer (UniFormer), which can seamlessly integrate the merits of convolution and self-attention in a concise transformer format. Different from the typical transformer blocks, the relation aggregators in our UniFormer block are equipped with local and global token affinity respectively in shallow and deep layers, allowing to tackle both redundancy and dependency for efficient and effective representation learning. Finally, we flexibly stack our UniFormer blocks into a new powerful backbone, and adopt it for various vision tasks from image to video domain, from classification to dense prediction. Without any extra training data, our UniFormer achieves **86.3** top-1 accuracy on ImageNet-1K classification. With only ImageNet-1K pre-training, it can simply achieve state-of-the-art performance in a broad range of downstream tasks, e.g., it obtains **82.9/84.8** top-1 accuracy on Kinetics-400/600, **60.9/71.2** top-1 accuracy on Something-Something V1/V2 video classification tasks, **53.8** box AP and **46.4** mask AP on COCO object detection task, **50.8** mIoU on ADE20K semantic segmentation task, and **77.4** AP on COCO pose estimation task. Code is available at <https://github.com/Sense-X/UniFormer>.

Index Terms—UniFormer, Convolution Neural Network, Transformer, Self-Attention, Visual Recognition.

1 INTRODUCTION

REPRESENTATION learning is a fundamental research topic for visual recognition [23], [56]. Basically, we confront two distinct challenges that exist in the visual data such as images and videos. On one hand, the local redundancy is large, e.g., visual content in a local region (space, time or space-time) tends to be similar. Such locality often introduces inefficient computation. On the other hand, the global dependency is complex, e.g., targets in different regions have dynamic relations. Such long-range interaction often causes ineffective learning.

To tackle such difficulties, researchers have proposed a number of powerful models in visual recognition [27], [96], [104], [105]. In particular, the mainstream backbones are Convolution Neural Networks (CNNs) [29], [35], [37] and Vision Transformers (ViTs) [23], [79], where convolution and self-attention are the key operations in these two structures. Unfortunately, each of these operations mainly addresses one aforementioned challenge while ignoring the other. For example, the convolution operation is good at reducing local redundancy and avoiding unnecessary computation, by aggregating each pixel with context from a small neighborhood (e.g, 3×3 or $3 \times 3 \times 3$). However, the limited receptive field makes convolution suffer from difficulty in learning global dependency [50], [90]. Alternatively, self-attention has been recently highlighted in the ViTs. By similarity comparison among visual tokens, it exhibits the strong capacity of learning global dependency in both images [23],

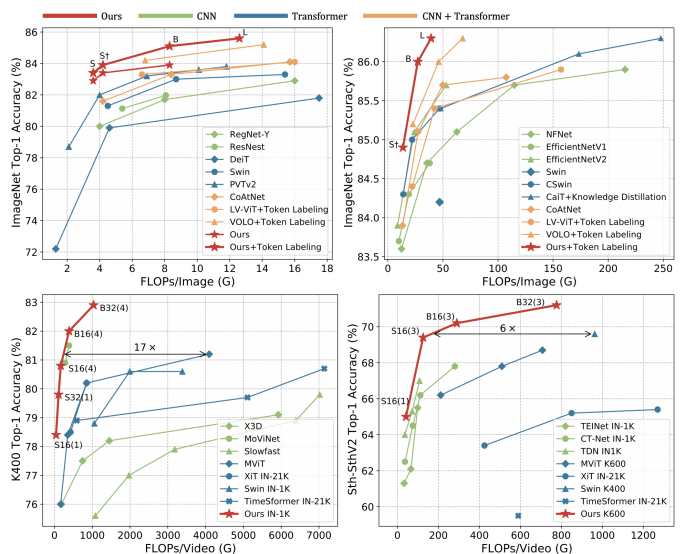


Fig. 1. Accuracy vs. GFLOPs per input. Top: Image Classification (Left/Right: ImageNet with resolution of $224 \times 224/384 \times 384$). Bottom: Video Classification (Left/Right: K400/Sth-SthV2). ‘(4)’ and ‘(3)’ mean we test UniFormer with 4 clips and 3 crops respectively (more testing details can be found in Section 5.6). Our UniFormer achieves the best balance between accuracy and computation on all the datasets.

[56] and videos [1], [3], [57]. Nevertheless, we observe that ViTs are often inefficient to encode local features in the shallow layers.

We take the well-known ViTs in the image and video domains (i.e., DeiT [78] and TimeSformer [3]) as examples, and visualize their attention maps in the shallow layer. As shown in Figure 2, both ViTs indeed capture detailed visual features in the shallow layer, while spatial and temporal attention are redundant. One can

- K. Li and Y. Wang are equally-contributed authors.
- K. Li, Y. Wang and Y. Qiao are with Shenzhen Institutes of Advanced Technology, Chinese Academy of Sciences. E-mail: {kc.li, yl.wang}@siat.ac.cn
- J. Zhang is with National University of Singapore, P. Gao and Y. Qiao are with Shanghai AI Laboratory, G. Song and Y. Liu are with SenseTime Research and H. Li is with the Chinese University of Hong Kong.
- Y. Qiao is the corresponding author. Email: qiaoyu@pjlab.org.cn

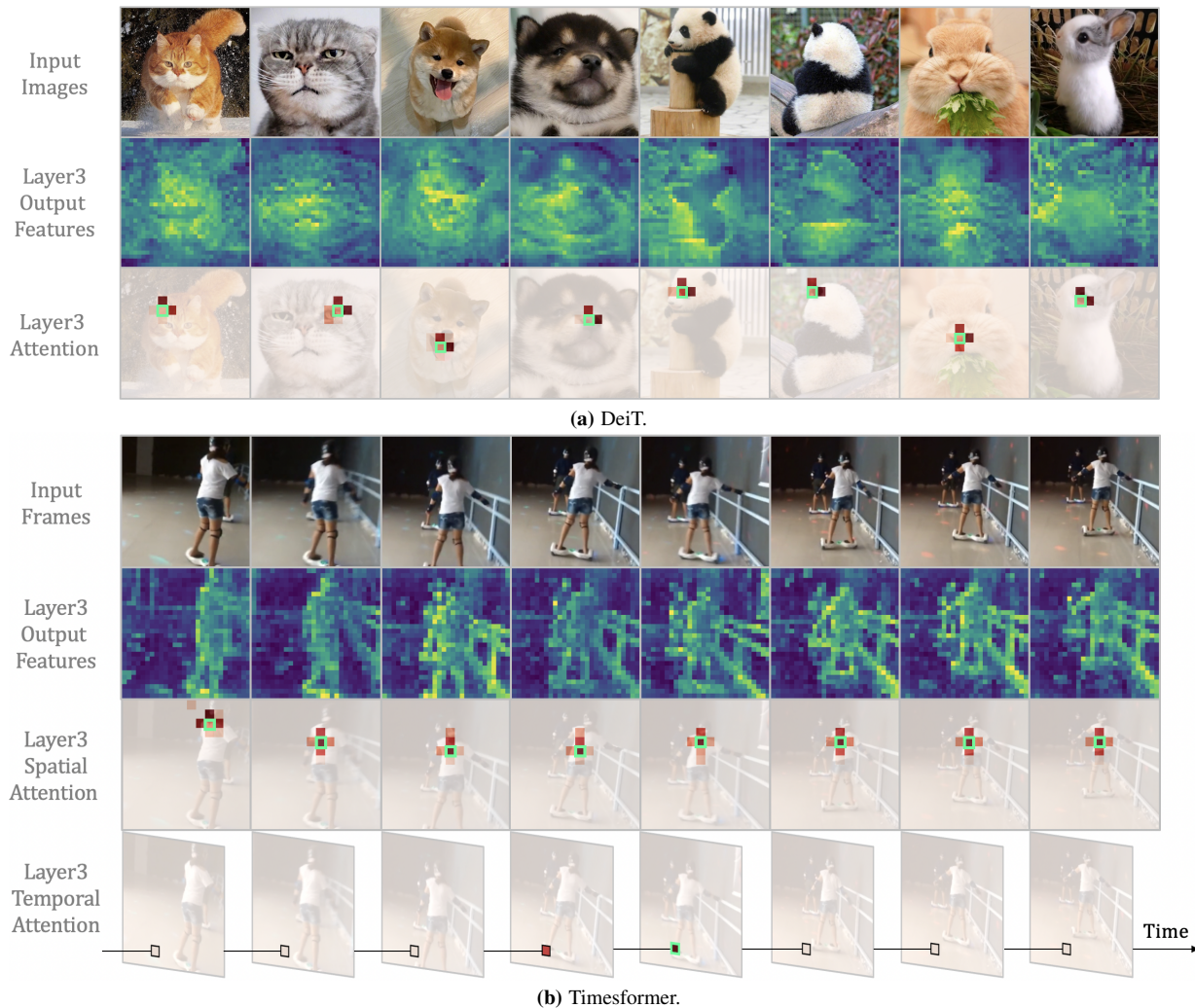


Fig. 2. Visualization of vision transformers. We take the well-known Vision Transformers (ViTs) in both image and video domains (i.e., DeiT [78] and TimeSformer [3]) for illustration, where we respectively show the feature maps, spatial and temporal attention maps from the 3rd layer of these ViTs. We find that, such ViTs learns local representations with redundant global attention. For an anchor token (green box), spatial/temporal attention compares it with all the contextual tokens for aggregation, while only its neighboring tokens (boxes filled with red color) actually work. Hence, ViTs spend large computation on encoding very local visual representations with global self-attention.

easily see that, given an anchor token, spatial attention largely concentrates on the tokens in the local region (mostly 3×3), and learns little from the rest tokens in this image. Similarly, temporal attention mainly aggregates the tokens in the adjacent frames, while losing sight of the rest tokens in the distant frames. However, such local focus is obtained by global comparison among all the tokens in space and time. Clearly, this redundant attention manner brings large and unnecessary computation burden, thus deteriorating the computation-accuracy balance in ViTs (Figure 1).

Based on these discussions, we propose a novel Unified transformer (UniFormer) in this work. It flexibly unifies convolution and self-attention in a concise transformer format, which can tackle both local redundancy and global dependency for effective and efficient visual recognition. Specifically, our UniFormer block consists of three key modules, i.e., Dynamic Position Embedding (DPE), Multi-Head Relation Aggregator (MHRA), and Feed-Forward Network (FFN). The distinct design of relation aggregator is the key difference between our UniFormer and the previous CNNs and ViTs. In the shallow layers, our relation aggregator captures local token affinity with a small learnable parameter matrix, which inherits the convolution style that can largely reduce

computation redundancy by context aggregation in the local region. In the deep layers, our relation aggregator learns global token affinity with token similarity comparison, which inherits the self-attention style that can adaptively build long-range dependency from distant regions or frames. Via progressively stacking local and global UniFormer blocks in a hierarchical manner, we can flexibly integrate their cooperative power to promote representation learning. Finally, we provide a generic and powerful backbone for visual recognition and successfully address various downstream vision tasks with simple and elaborate adaptation.

Extensive experiments demonstrate the strong performance of our UniFormer on a broad range of vision tasks, including image classification, video classification, object detection, instance segmentation, semantic segmentation and pose estimation. Without any extra training data, UniFormer-L achieves **86.3** top-1 accuracy on ImageNet-1K. Moreover, with only ImageNet-1K pre-training, UniFormer-B achieves **82.9/84.8** top-1 accuracy on Kinetics-400/Kinetics-600, **60.9** and **71.2** top-1 accuracy on Something-400/kinetics-600, **53.8** box AP and **46.4** mask AP on the COCO detection task, **50.8** mIoU on the ADE20K semantic segmentation task, and **77.4** AP on the COCO pose estimation task.

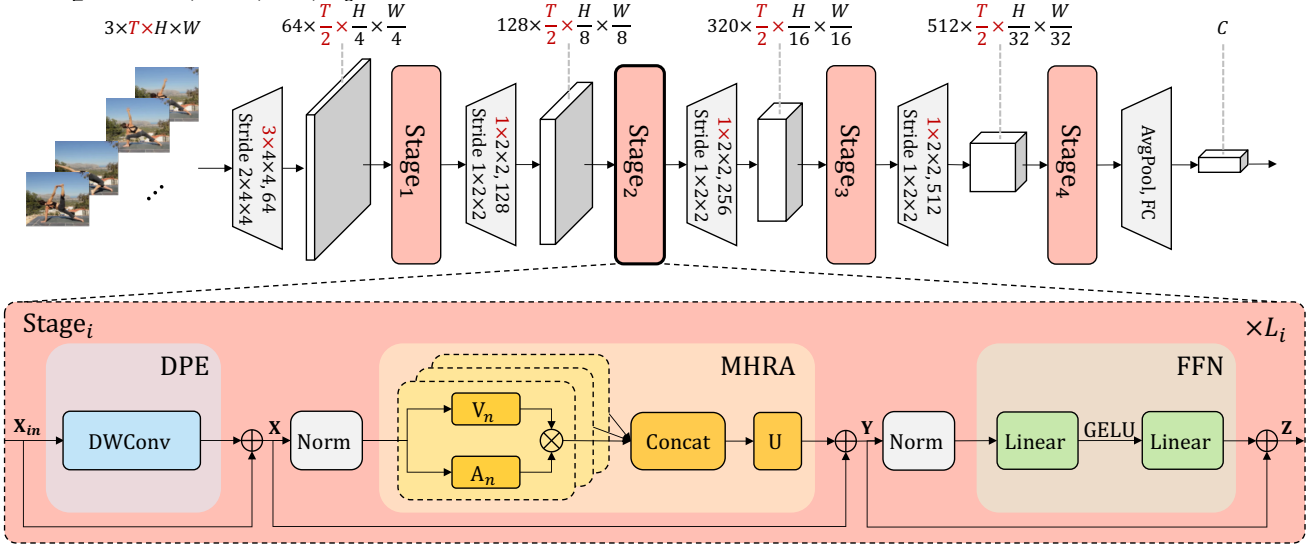


Fig. 3. Unified transFormer (UniFormer). A UniFormer block consists of three key modules, i.e., Dynamic Position Embedding (DPE), Multi-Head Relation Aggregator (MHRA), and Feed Forward Network (FFN). The dimensions highlighted in red only exist for the video input, while all of them are equal to one for an image input. More detailed explanations can be found in Section 3.

2 RELATED WORK

2.1 Convolution Neural Networks (CNNs)

Beginning with AlexNet [46], convolutional neural networks (CNNs) have dominated a broad range of vision tasks [21], [55], [109]. In the past few years, more and more effective CNNs have been proposed and achieved great success in the image understanding, including VGG [72], Inception [75], ResNet [35], ResNeXt [96], DenseNet [38], MobileNet [37], ShuffleNet [108] and EfficientNet [76]. As for video understanding, it is natural to apply 3D convolution on a stack of frames [80]. However, 3D CNNs suffer from difficult optimization problem and large computation cost. To resolve these issues, the prior works try to inflate the pre-trained 2D convolution kernels for better optimization [11] and factorize the 3D convolution kernels in different dimensions to reduce complexity [28], [29], [65], [81], [82]. Additionally, other studies [41], [49], [50], [52], [54] focus on enhancing the temporal modeling ability for 2D CNNs via well-designed plug-and-play modules, such as temporal shift [54], [62], motion enhancement [41], [52], [58] and spatiotemporal excitation [49], [50]. Unfortunately, due to the limited reception field, typical spatial and temporal convolution struggle to capture long-range dependency even if stacked deeper.

2.2 Vision Transformers (ViTs)

Inspired by the success of self-attention mechanism and Transformer architectures in NLP, Vision Transformer (ViT) applies pure Transformer encoder to encode a sequence of image tokens, achieving competitive superior performance to CNNs with sufficient data and detailed data augmentation. Following works mainly concentrates on improve ViT from different perspectives, such as improved patch embedding [51], data-efficient training [78], efficient self-attention [22], [56], [97] and multi-scale architectures [27], [89]. Besides, many efforts have been devoted to applying ViTs for various vision tasks, including object detection [8], [111], semantic segmentation [14], [43], [95], pose estimation [51], [98], [102], re-identification [36], and low-level image processing [12], [53]. Furthermore, other works propose different variants for spatiotemporal representation learning [1], [3], [5], [27], [57], [64], such as video object tracking [88], video object segmentation [24],

video retrieval [25], [30] and video super-resolution [7]. These results verify the outstanding ability of the transformer to capture long-term information. However, the self-attention mechanism is inefficient to encode low-level features, hindering their high potential for efficient representation learning.

2.3 Combination of CNN and ViT

The prior works have demonstrate that self-attention can perform convolution [19], [68], but they suggest replacing convolution instead of combining them. Current combination of CNN and ViT mainly focus on image understanding, which try to enhance ViTs with convolution in different ways, e.g., adding convolutional patch stem for fast convergence [94], [99], introducing convolutional position embedding [16], [22], inserting depthwise convolution into feed-forward network to encode local features [99], [102], utilizing squeezed convolutional projection to reduce computation [91] and combining MBCov [69] with Transformer [20]. However, the above works lack analysis for the representation learning ability and property of convolution and self-attention. As for video understanding, the combination is almost straightforward, e.g., inserting self-attention as global attention [90] or using convolution as patch stem [59]. Though Video Swin [57] advocates an inductive bias of locality with shift window, it is inefficient to encode low-level features via self-attention. In this work, we analyze the learning features of pure self-attention and the relation between convolution and self-attention, thus we propose a unified relation aggregator to form our effective backbone for visual recognition.

3 METHOD

In this section, we introduce the proposed UniFormer in detail. First, we describe the overview of our UniFormer block. Then, we explain its key modules such as multi-head relation aggregator and dynamic position embedding. Moreover, we discuss the distinct relations between our UniFormer and existing convolution/transformer blocks, showing its preferable design for accuracy-computation balance. Finally, we stack UniFormer blocks hierarchically to build up our backbone for visual recognition, and propose an effective adaption for various downstream vision tasks.

3.1 Overview

Figure 3 shows our concise Unified transFormer (UniFormer). For simple description, we take a video with T frames as an example and an image input can be seen as a video with a single frame. Hence, the dimensions highlighted in red only exit for the video input, while all of them are equal to one for image input. One can see that, our UniFormer is a basic transformer format, while we elaborately design it to tackle computational redundancy and capture complex dependency.

Specifically, our UniFormer block consist of three key modules: Dynamic Position Embedding (DPE), Multi-Head Relation Aggregator (MHRA) and Feed-Forward Network (FFN):

$$\mathbf{X} = \text{DPE}(\mathbf{X}_{in}) + \mathbf{X}_{in}, \quad (1)$$

$$\mathbf{Y} = \text{MHRA}(\text{Norm}(\mathbf{X})) + \mathbf{X}, \quad (2)$$

$$\mathbf{Z} = \text{FFN}(\text{Norm}(\mathbf{Y})) + \mathbf{Y}. \quad (3)$$

Considering the input token tensor $\mathbf{X}_{in} \in \mathbb{R}^{C \times T \times H \times W}$ ($T = 1$ for an image input), we first introduce DPE to dynamically integrate position information into all the tokens (Eq. 1). It is friendly to arbitrary input resolution and makes good use of token order for better visual recognition. Then, we use MHRA to enhance each token by exploiting its contextual tokens with relation learning (Eq. 2). Via flexibly designing the token affinity in the shallow and deep layers, our MHRA can smartly unify convolution and self-attention to reduce local redundancy and learn global dependency. Finally, we add FFN like traditional ViTs [23], which consists of two linear layers and one non-linear function, i.e., GELU (Eq. 3). The channel number is first expanded by the ratio of 4 and then recovered, thus each token will be enhanced individually.

3.2 Multi-Head Relation Attention

As analyzed before, the traditional CNNs and ViTs focus on addressing either local redundancy or global dependency, leading to unsatisfactory accuracy or/and unnecessary computation. To overcome these difficulties, we introduce a generic Relation Aggregator (RA), which elegantly unifies convolution and self-attention as token relation learning. It can achieve efficient and effective representation learning by designing local and global token affinity in the shallow and deep layers respectively. Specifically, MHRA exploits token relationships in a multi-head style:

$$\mathbf{R}_n(\mathbf{X}) = \mathbf{A}_n \mathbf{V}_n(\mathbf{X}), \quad (4)$$

$$\text{MHRA}(\mathbf{X}) = \text{Concat}(\mathbf{R}_1(\mathbf{X}); \mathbf{R}_2(\mathbf{X}); \dots; \mathbf{R}_N(\mathbf{X}))\mathbf{U}. \quad (5)$$

Given the input tensor $\mathbf{X} \in \mathbb{R}^{C \times T \times H \times W}$ ($T = 1$ for an image input), we first reshape it to a sequence of tokens $\mathbf{X} \in \mathbb{R}^{L \times C}$ with the length of $L = T \times H \times W$. Moreover, $\mathbf{R}_n(\cdot)$ refers to RA in the n -th head and $\mathbf{U} \in \mathbb{R}^{C \times C}$ is a learnable parameter matrix to integrate N heads. Each RA consists of token context encoding and token affinity learning. We apply a linear transformation to encode the original tokens into contextual tokens $\mathbf{V}_n(\mathbf{X}) \in \mathbb{R}^{L \times \frac{C}{N}}$. Subsequently, RA can summarize context with the guidance of token affinity $\mathbf{A}_n \in \mathbb{R}^{L \times L}$. We will describe how to learn the specific \mathbf{A}_n in the following.

3.2.1 Local MHRA

As shown in Figure 2, though the previous ViTs compare similarities among all the tokens, they finally learn local representations. Such redundant self-attention design brings large computation cost in the shallow layers. Based on this observation, we suggest learning token affinity in a small neighborhood, which coinciden-

tally shares a similar insight with the design of a convolution filter. Hence, we propose to represent local affinity as a learnable parameter matrix in the shallow layers. Concretely, given an anchor token \mathbf{X}_i , our local RA learns the affinity between this token and other tokens in the small neighborhood $\Omega_i^{t \times h \times w}$ ($t = 1$ for an image input):

$$\mathbf{A}_n^{local}(\mathbf{X}_i, \mathbf{X}_j) = a_n^{i-j}, \quad \text{where } j \in \Omega_i^{t \times h \times w}, \quad (6)$$

where $a_n \in \mathbb{R}^{t \times h \times w}$ and \mathbf{X}_j refers to any neighbor token in $\Omega_i^{t \times h \times w}$. $(i - j)$ denotes the relative position between token i and j . Note that, visual content between adjacent tokens varies subtly in the shallow layers, since the receptive field of tokens is small. In this case, it is not necessary to make token affinity dynamic in these layers. Hence, we use a learnable parameter matrix to describe local token affinity, which simply depends on the relative position between tokens.

Comparison to Convolution Block. Interestingly, we find that our local MHRA can be interpreted as a generic extension of MobileNet block [28], [69], [81]. Firstly, the linear transformation $\mathbf{V}(\cdot)$ in Eq. 4 is equivalent to a pointwise convolution (PWConv), where each head is corresponding to an output feature channel $\mathbf{V}_n(\mathbf{X})$. Furthermore, our local token affinity \mathbf{A}_n^{local} can be instantiated as the parameter matrix that operated on each output channel (or head) $\mathbf{V}_n(\mathbf{X})$, thus the relation aggregator $\mathbf{R}_n(\mathbf{X}) = \mathbf{A}_n^{local} \mathbf{V}_n(\mathbf{X})$ can be explained as a depthwise convolution (DWConv). Finally, the linear matrix \mathbf{U} , which concatenates and fuses all heads, can also be seen as a pointwise convolution. As a result, such local MHRA can be reformulated with a manner of PWConv-DWConv-PWConv in the MobileNet block. In our experiments, we instantiate our local MHRA as such channel-separated convolution, so that our UniFormer can boost computation efficiency for visual recognition. Moreover, different from the MobileNet block, our local UniFormer block is designed as a generic transformer format, i.e., it also contains dynamical position encoding (DPE) and feed-forward network (FFN), besides MHRA. This unique integration can effectively enhance token representation, which has not been explored in the previous convolution blocks.

3.2.2 Global MHRA

In the deep layers, it is important to exploit long-range relation in the broader token space, which naturally shares a similar insight with the design of self-attention. Therefore, we design the token affinity via comparing content similarity among all the tokens in the global view:

$$\mathbf{A}_n^{global}(\mathbf{X}_i, \mathbf{X}_j) = \frac{e^{Q_n(\mathbf{X}_i)^T K_n(\mathbf{X}_j)}}{\sum_{j' \in \Omega_{T \times H \times W}} e^{Q_n(\mathbf{X}_i)^T K_n(\mathbf{X}_{j'})}}, \quad (7)$$

where \mathbf{X}_j can be any token in the global tube with a size of $T \times H \times W$ ($T = 1$ for an image input), while $Q_n(\cdot)$ and $K_n(\cdot)$ are two different linear transformations.

Comparison to Transformer Block. Our global MHRA \mathbf{A}_n^{global} (Eq. 7) can be instantiated as a spatiotemporal self attention, where $Q_n(\cdot)$, $K_n(\cdot)$ and $V_n(\cdot)$ become Query, Key and Value in ViT [23]. Hence, it can effectively learn long-range dependency. However, our global UniFormer block is different from the previous ViT blocks. First, most video transformers divide spatial and temporal attention in the video domain [1], [3], [71], in order to reduce the dot-product computation in token similarity comparison. But such an operation inevitably deteriorates the spatiotemporal relation among tokens. In contrast, our global UniFormer block

| Model | Type | #Blocks | #Channels | #Param. | FLOPs |
|-------|--------------|----------------|----------------------|---------|-------|
| Small | [L, L, G, G] | [3, 4, 8, 3] | [64, 128, 320, 512] | 21.5M | 3.6G |
| Base | [L, L, G, G] | [5, 8, 20, 7] | [64, 128, 320, 512] | 50.3M | 8.3G |
| Large | [L, L, G, G] | [5, 10, 24, 7] | [128, 192, 448, 640] | 100M | 12.6G |

TABLE 1. Backbones for image classification. ‘L’ and ‘G’ refer to our local and global UniFormer blocks respectively. Backbones for Image Classification. The FLOPs are measured at resolution 224×224 .

jointly encodes spatiotemporal token relation to generate more discriminative video representation for recognition. Since our local UniFormer block largely saves computation of token comparison in the shallow layers, the overall model can achieve a preferable computation-accuracy balance. Second, instead of absolute position embedding [23], [83], we adopt dynamic position embedding (DPE) in our UniFormer. It is in convolution style (see the next section), which can overcome permutation-invariance and be friendly to different input lengths of visual tokens.

3.3 Dynamic Position Embedding

The position information is an important clue to describe visual representation. Previously, most ViTs encode such information by absolute or relative position embedding [23], [56], [89]. However, absolute position embedding has to be interpolated for various input sizes with fine-tuning [78], [79], while relative position embedding does not work well due to the modification of self-attention [16]. To improve flexibility, convolutional position embedding has been recently proposed [15], [22]. In particular, conditional position encoding (CPE) [16] can implicitly encode position information via convolution operators, which unlocks Transformer to process arbitrary input size and promotes recognition performance. Due to its plug-and-play property, we flexibly adopt it as our Dynamical Position Embedding (DPE) in the UniFormer:

$$\text{DPE}(\mathbf{X}_{in}) = \text{DWConv}(\mathbf{X}_{in}), \quad (8)$$

where DWConv refers to depthwise convolution with zero paddings. We choose such a design as our DPE based on the following reasons. First, depthwise convolution is friendly to arbitrary input shapes, e.g., it is straightforward to use its spatiotemporal version to encode 3D position information in videos. Second, depthwise convolution is light-weight, which is an important factor for computation-accuracy balance. Finally, we add extra zero paddings, since it can help tokens be aware of their absolute positions by querying their neighbors progressively [16].

4 FRAMEWORK

In the section, we mainly develop visual frameworks for various downstream tasks. Specifically, we first develop a number of visual backbones for image classification, by hierarchically stacking our local and global UniFormer blocks with consideration of computation-accuracy balance. Then, we extend the above backbones to tackle other representative vision tasks, including video classification and dense prediction (i.e., object detection, semantic segmentation and human pose estimation). Such generality and flexibility of our UniFormer demonstrate its valuable potential for computer vision research and beyond.

4.1 Image Classification

It is important to progressively learn visual representation for capturing semantics in the image. Hence, we build up our backbone with four stages, as illustrated in Figure 3.

More specifically, we use the local UniFormer blocks in the first two stages to reduce computation redundancy, while the global

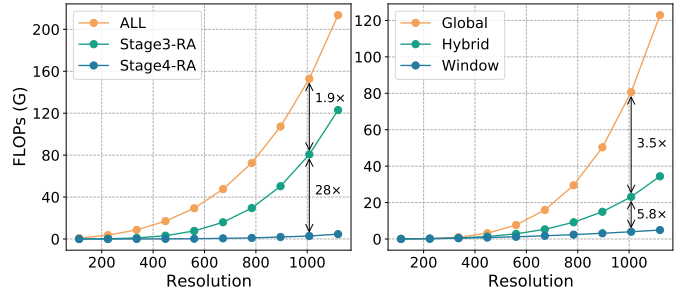


Fig. 4. FLOPs vs. Resolution. **Left:** Total FLOPs and the FLOPs of MatMul in RA in Stage3 and Stage4. RA in Stage3 requires huge computation for large resolution. **Right:** The FLOPs of MatMul in different RA in Stage3. Window and hybrid blocks saves computation.

UniFormer blocks are utilized in the last two stages to learn long-range token dependency. For the local UniFormer block, MHRA is instantiated as PWConv-DWConv-PWConv with local token affinity (Eq. 6), where the spatial size of DWConv is set to 5×5 for image classification. For the global UniFormer block, MHRA is instantiated as multi-head self-attention with global token affinity (Eq. 7), where the number of attention heads is set to 64. For both local and global UniFormer blocks, DPE is instantiated as DWConv with a spatial size of 3×3 , and the expand ratio of FFN is 4.

Additionally, as suggested in the CNN and ViT literatures [23], [35], we utilize BN [40] for convolution and LN [2] for self attention. For feature downsampling, we use the 4×4 convolution with stride 4×4 before the first stage and the 2×2 convolution with stride 2×2 before other stages. Besides, an extra LN is added after each downsampling convolution. Finally, the global average pooling and fully connected layer are applied to output the predictions. Note that when training models with Token Labeling [42], we add another fully connected layer for auxiliary loss. To satisfy various computation requirement, we design three model variants in Table 1.

4.2 Video Classification

Given our image-based 2D backbones, one can easily adapt them as 3D backbones for video classification. Without loss of generality, we adjust Small and Base models for spatiotemporal modeling. Specifically, the model architectures keep the same with four stages, where we use the local UniFormer blocks in the first two stages and the global UniFormer blocks in the last two stages. But differently, all the 2D convolution filters are changed as 3D ones via filter inflation [11]. Concretely, the kernel size of DWConv in DPE and local MHRA are $3 \times 3 \times 3$ and $5 \times 5 \times 5$ respectively. Specially, we downsample both spatial and temporal dimensions before the first stage. Hence, the convolution filter before this stage becomes $3 \times 4 \times 4$ with stride of $2 \times 4 \times 4$. For the other stages, we just downsample the spatial dimension to decrease the computation cost and maintain high performance. Hence, the convolution filters before these stages are $1 \times 2 \times 2$ with stride of $1 \times 2 \times 2$.

Note that we use spatiotemporal attention in the global UniFormer blocks for learning token relation jointly in the 3D view. It is worth mentioning that, due to the large model sizes, the previous video transformers [1], [3] divide spatial and temporal attention to reduce computation and alleviate overfitting, but such factorization operation inevitably tears spatiotemporal token relations. In contrast, our joint spatiotemporal attention can avoid the issue. Besides, since our local UniFormer blocks largely save computation via 3D DWconv, our model can achieve effective and efficient video representation learning.

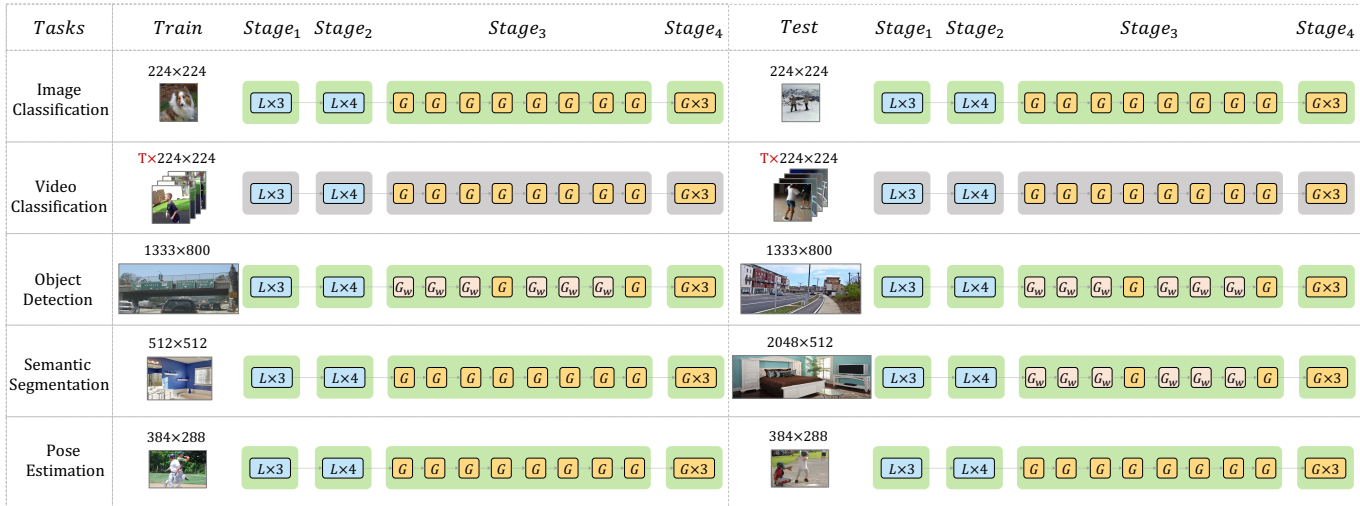


Fig. 5. Training and testing adaption for downstream tasks. For video classification, we inflate all the 2D convolution filters to 3D ones. For dense prediction, we modify RA in Stage3 for different downstream tasks. ‘ G_w ’ means we apply global MHRA in a predefined window.

4.3 Dense Prediction

Dense prediction tasks are necessary to verify the generality of our recognition backbones. Hence, we adopt our UniFormer backbones for a number of popular dense tasks such as object detection, instance segmentation, semantic segmentation, and human pose estimation. However, direct usage of our backbone is not suitable because of the high input resolution of most dense prediction tasks, e.g., the size of the image is 1333×800 in the COCO object detection dataset. Naturally, feeding such image into our classification backbones would inevitably lead to large computation, especially when operating self-attention of global UniFormer block in the last two stages. Taking $h \times w$ visual tokens as an example, the MatMul operation in token similarity comparison (Eq. 7) causes $\mathcal{O}(w^2h^2)$ complexity, which is prohibitive for most dense tasks.

For this reason, we propose to adjust the global UniFormer block for different downstream tasks. First, we analyze the FLOPs of our UniFormer-S under different input resolutions. As shown in Figure 4, it clearly indicates that Relation Aggregator (RA) in Stage3 occupies large computation, e.g., for a 1008×1008 image, the MatMul operation of RA in Stage3 even occupies over 50% of the total FLOPs of UniFormer-S, while the FLOPs in Stage4 is only 1/28 of that in Stage3. Therefore, we mainly modify RA in Stage3 for computation reduction.

Inspired by [56], [68], we propose to apply our global MHRA in a predefined window (e.g., 14×14), instead of using it in the entire image with high resolution. Such operation can effectively cut down computation with complexity of $\mathcal{O}(whp^p)$, where p is the window size. However, it undoubtedly drops model performance, due to insufficient token interaction. To bridge such a gap, we integrate window and global UniFormer blocks together in Stage3, where a hybrid group consists of three window blocks and one global block. In this case, there are 2/5 hybrid groups in Stage3 of our UniFormer-Small/Base backbones.

Based on this design, we next introduce the specific backbone settings of various dense tasks, depending on the input resolution of training and testing images. For object detection and instance segmentation, the input images are usually large (e.g., 1333×800), thus we adopt the hybrid block style in Stage3. In contrast, the inputs are relatively small for pose estimation, such as 384×288 , hence global blocks are still applied in Stage3 for both training and testing. Specially, for semantic segmentation, the testing images are

often larger than the training ones. Therefore, we utilize the global blocks in Stage3 for training, while adapting the hybrid blocks in Stage3 for testing. In particular, we use the following simple design: the window-based block in testing has the same receptive field as the global block in training, e.g., 32×32 . Such design can maintain training efficiency, and boost testing performance by keeping consistency with training as much as possible.

5 EXPERIMENTS

To verify effectiveness and efficiency of our UniFormer for visual recognition, we conduct extensive experiments on ImageNet-1K [21] image classification, Kinetics-400 [10]/600 [9] and Something-Something V1&V2 [33] video classification, COCO [55] object detection, instance segmentation and pose estimation, and ADE20K [109] semantic segmentation. We also perform comprehensive ablation studies to analyze each design of our UniFormer.

5.1 Image Classification

5.1.1 Settings

We train our models from scratch on the ImageNet-1K dataset [21]. For a fair comparison, we follow the same training strategy proposed in DeiT [78] by default, including the strong data augmentation and regularization. Additionally, we set stochastic depth rate as 0.1/0.3/0.4 respectively for our UniFormer-S/B/L in Table 1. We train all models via AdamW [60] optimizer with cosine learning rate schedule [61] for 300 epochs, while the first 5 epochs are utilized for linear warm-up [32]. The weight decay, learning rate and batch size are set to 0.05, $1e-3$ and 1024 respectively. For UniFormer-S†, we followed state-of-the-art ViTs [22], [97] to apply overlapped patch embedding and blocks (3/5/9/3 blocks in each stage) for fair comparisons. As for UniFormer-B, we use the learning rate of $8e-4$ for better convergence.

For training high-performance ViTs, hard distillation [78] and Token Labeling [42] are proposed, both of which are complementary to our backbones. Since Token Labeling is more efficient, we apply it with an extra fully connected layer and auxiliary loss, following the settings in LV-ViT [42]. Different from the training settings in DeiT, MixUp [106] and CutMix [103] are not used since they conflict with MixToken [42]. The base learning rate is $1.6e-3$ for the batch size of 1024 by default. Specially, we adopt the base learning rate of $1.2e-3$ and layer scale [79] for UniFormer-L to

avoid NaN loss. When fine-tuning our models on larger resolution, i.e., 384×384 , the weight decay, learning rate, batch size, warm-up epoch and total epoch are set to $1e-8$, $5e-6$, 512, 5 and 30.

5.1.2 Results

In Table 2, we compare our UniFormer with the state-of-the-art CNNs, ViTs and their combinations. It clearly shows that our UniFormer outperforms previous models under different computation restrictions. For example, our UniFormer-S[†] achieves 83.4% top-1 accuracy with only 4.2G FLOPs, surpassing RegNetY-4G [67], Swin-T [56], CSwin-T [22] and CoAtNet [20] by 3.4%, 2.1%, 0.7% and 1.8% respectively. Though EfficientNet [76] comes from extensive neural architecture search, our UniFormer outperforms it (83.9% vs. 83.6%) with less computation cost (8.3G vs. 9.9G).

We further enhance our models with Token Labeling [42], which is labeled by ‘*’. Compared with the models training with the same settings, our UniFormer-L achieves higher accuracy but only 21% FLOPs of LV-ViT-M [42] and 61% FLOPs of VOLO-D3 [101]. Moreover, when fine-tuned on 384×384 images, our UniFormer-L obtains 86.3% top-1 accuracy. It is even better than EfficientNetV2-L [77] with larger input, demonstrating the powerful learning capacity of our UniFormer.

5.2 Video Classification

5.2.1 Settings

We evaluate our UniFormer on the popular Kinetics-400 [10] and Kinetics-600 [9], and we verify the transfer learning performance on temporal-related datasets Something-Something V1&V2 [33]. Our codes mainly rely on PySlowFast [26]. For training, we adopt the same training strategy as MViT [27] by default, but we do not apply random horizontal flip for Something-Something. We utilize AdamW [60] optimizer with cosine learning rate schedule [61] to train our video backbones. The first 5 or 10 epochs are used for warm-up [32] to overcome early optimization difficulty. For UniFormer-S, the warmup epoch, total epoch, stochastic depth rate, weight decay are set to 10, 110, 0.1 and 0.05 respectively for Kinetics and 5, 50, 0.3 and 0.05 respectively for Something-Something. For UniFormer-B, all the hyper-parameters are the same unless the stochastic depth rates are doubled. Moreover, We linearly scale the base learning rates according to the batch size, which are $1e-4 \cdot \frac{batchsize}{32}$ and $2e-4 \cdot \frac{batchsize}{32}$ for Kinetics and Something-Something respectively.

We utilize the dense sampling strategy [90] for Kinetics and uniform sampling strategy [86] for Something-Something. To reduce the total training cost, we inflate the 2D convolution kernels pre-trained on ImageNet for Kinetics [11]. To obtain a preferable computation-accuracy balance, we adopt multi-clip testing for Kinetics and multi-crop testing for Something-Something. All scores are averaged for the final prediction.

5.2.2 Results on Kinetics

In Table 3, we compare our UniFormer with the state-of-the-art methods on Kinetics-400 and Kinetics-600. The first part shows the prior works using CNN. Compared with SlowFast [29] equipped with non-local blocks [90], our UniFormer-S_{16f} requires $42 \times$ fewer GFLOPs but obtains 1.0% performance gain on both datasets (80.8% vs. 79.8% and 82.8% vs. 81.8%). Even compared with MoViNet [45], which is a strong CNN-based models via extensive neural architecture search, our model achieves slightly better results (82.0% vs. 81.5%) with fewer input frames ($16f \times 4$ vs.

| Arch. | Method | #Param (M) | FLOPs (G) | Train Size | Test Size | ImageNet Top-1 |
|---|--------------------------------|------------|-----------|------------|-------------|----------------|
| CNN | RegNetY-4G [67] | 21 | 4.0 | 224 | 224 | 80.0 |
| | EfficientNet-B5 [76] | 30 | 9.9 | 456 | 456 | 83.6 |
| | EfficientNetV2-S [77] | 22 | 8.5 | 384 | 384 | 83.9 |
| Trans | DeiT-S [78] | 22 | 4.6 | 224 | 224 | 79.9 |
| | PVT-S [89] | 25 | 3.8 | 224 | 224 | 79.8 |
| | T2T-14 [100] | 22 | 5.2 | 224 | 224 | 80.7 |
| | Swin-T [56] | 29 | 4.5 | 224 | 224 | 81.3 |
| | Focal-T [97] | 29 | 4.9 | 224 | 224 | 82.2 |
| | CSwin-T [22] | 23 | 4.3 | 224 | 224 | 82.7 |
| | CSwin-T $\uparrow 384$ [22] | 23 | 14.0 | 224 | 384 | 84.3 |
| CNN+Trans | CvT-13 [91] | 20 | 4.5 | 224 | 224 | 81.6 |
| | CvT-13 $\uparrow 384$ [91] | 20 | 16.3 | 224 | 384 | 83.0 |
| | CoAtNet-0 [20] | 25 | 4.2 | 224 | 224 | 81.6 |
| | CoAtNet-0 $\uparrow 384$ [20] | 20 | 13.4 | 224 | 384 | 83.9 |
| | Container [31] | 22 | 8.1 | 224 | 224 | 82.7 |
| | LV-ViT-S [42] | 26 | 6.6 | 224 | 224 | 83.3 |
| | LV-ViT-S $\uparrow 384$ [42] | 26 | 22.2 | 224 | 384 | 84.4 |
| | UniFormer-S | 22 | 3.6 | 224 | 224 | 82.9 |
| | UniFormer-S* | 22 | 3.6 | 224 | 224 | 83.4 |
| | UniFormer-S* $\uparrow 384$ | 22 | 11.9 | 224 | 384 | 84.6 |
| | UniFormer-S [†] | 24 | 4.2 | 224 | 224 | 83.4 |
| UniFormer-S [†] * | 24 | 4.2 | 224 | 224 | 83.9 | |
| UniFormer-S [†] * $\uparrow 384$ | 24 | 13.7 | 224 | 384 | 84.9 | |
| CNN | RegNetY-8G [67] | 39 | 8.0 | 224 | 224 | 81.7 |
| | EfficientNet-B7 [76] | 66 | 39.2 | 600 | 600 | 84.3 |
| | EfficientNetV2-M [77] | 54 | 25.0 | 480 | 480 | 85.1 |
| Trans | PVT-L [89] | 61 | 9.8 | 224 | 224 | 81.7 |
| | T2T-24 [100] | 64 | 13.2 | 224 | 224 | 82.2 |
| | Swin-S [56] | 50 | 8.7 | 224 | 224 | 83.0 |
| | Focal-S [97] | 51 | 9.1 | 224 | 224 | 83.5 |
| | CSwin-S [22] | 35 | 6.9 | 224 | 224 | 83.6 |
| | CSwin-S $\uparrow 384$ [22] | 35 | 22.0 | 224 | 384 | 85.0 |
| CNN+Trans | CvT-21 [91] | 32 | 7.1 | 224 | 224 | 82.5 |
| | CoAtNet-1 [20] | 42 | 8.4 | 224 | 224 | 83.3 |
| | CoAtNet-1 $\uparrow 384$ [20] | 42 | 27.4 | 224 | 384 | 85.1 |
| | LV-ViT-M [42] | 56 | 16.0 | 224 | 224 | 84.1 |
| | LV-ViT-M $\uparrow 384$ [42] | 56 | 42.2 | 224 | 384 | 85.4 |
| | UniFormer-B | 50 | 8.3 | 224 | 224 | 83.9 |
| UniFormer-B* | 50 | 8.3 | 224 | 224 | 85.1 | |
| UniFormer-B* $\uparrow 384$ | 50 | 27.2 | 224 | 384 | 86.0 | |
| CNN | RegNetY-16G [67] | 84 | 16.0 | 224 | 224 | 82.9 |
| | EfficientNetV2-L [77] | 121 | 53 | 480 | 480 | 85.7 |
| | NFNet-F4 [4] | 316 | 215.3 | 384 | 512 | 85.9 |
| Trans | DeiT-B [78] | 86 | 17.5 | 224 | 224 | 81.8 |
| | Swin-B [56] | 88 | 15.4 | 224 | 224 | 83.3 |
| | Swin-B $\uparrow 384$ | 88 | 47.0 | 224 | 384 | 84.2 |
| | Focal-B [56] | 90 | 16.0 | 224 | 224 | 83.8 |
| | CSwin-B [22] | 78 | 15.0 | 224 | 224 | 84.2 |
| | CSwin-B $\uparrow 384$ [22] | 78 | 47.0 | 224 | 384 | 85.4 |
| | CaiT-S36 $\uparrow 384$ Y [79] | 68 | 48.0 | 224 | 384 | 85.4 |
| | CaiT-M36 $\uparrow 448$ Y [79] | 271 | 247.8 | 224 | 448 | 86.3 |
| CNN+Trans | BoTNet-T7 [73] | 79 | 19.3 | 256 | 256 | 84.2 |
| | CoAtNet-3 [20] | 168 | 34.7 | 224 | 224 | 84.5 |
| | CoAtNet-3 $\uparrow 384$ [20] | 168 | 107.4 | 224 | 384 | 85.8 |
| | LV-ViT-L [42] | 150 | 59.0 | 288 | 288 | 85.3 |
| | LV-ViT-L $\uparrow 448$ [42] | 150 | 157.2 | 288 | 448 | 85.9 |
| | VOLO-D3 [101] | 86 | 20.6 | 224 | 224 | 85.4 |
| | VOLO-D3 $\uparrow 448$ [101] | 86 | 67.9 | 224 | 448 | 86.3 |
| UniFormer-L* | 100 | 12.6 | 224 | 224 | 85.6 | |
| UniFormer-L* $\uparrow 384$ | 100 | 39.2 | 224 | 384 | 86.3 | |

TABLE 2. Comparison with the state-of-the-art on ImageNet. ‘*’ means Token Labeling proposed in LV-ViT [42]. ‘Y’ means using RegNet-16GF [67] as teacher. For UniFormer-S[†], we apply overlapped patch embedding and more blocks for fair comparison.

| Method | Pretrain | #Frame | FLOPs (G) | K400 | | K600 | |
|-----------------------------|----------|-------------|--------------|-------------|-------|-------------|-------------|
| | | | | Top-1 | Top-5 | Top-1 | Top-5 |
| SmallBig _{EN} [50] | IN-1K | (8+32)×3×4 | 5700 | 78.7 | 93.7 | - | - |
| TDN _{EN} [87] | IN-1K | (8+16)×3×10 | 5940 | 79.4 | 94.4 | - | - |
| CT-Net _{EN} [49] | IN-1K | (16+16)×3×4 | 2641 | 79.8 | 94.2 | - | - |
| LGD [66] | IN-1K | 128×N/A | N/A | 79.4 | 94.4 | 81.5 | 95.6 |
| SlowFast [29] | - | 8×3×10 | 3180 | 77.9 | 93.2 | 80.4 | 94.8 |
| SlowFast+NL [29] | - | 16×3×10 | 7020 | 79.8 | 93.9 | 81.8 | 95.1 |
| ip-CSN [81] | Sports1M | 32×3×10 | 3270 | 79.2 | 93.8 | - | - |
| CorrNet [84] | Sports1M | 32×3×10 | 6720 | 81.0 | - | - | - |
| X3D-M [28] | - | 16×3×10 | 186 | 76.0 | 92.3 | 78.8 | 94.5 |
| X3D-XL [28] | - | 16×3×10 | 1452 | 79.1 | 93.9 | 81.9 | 95.5 |
| MoViNet-A5 [45] | - | 120×1×1 | 281 | 80.9 | 94.9 | 82.7 | 95.7 |
| MoViNet-A6 [45] | - | 120×1×1 | 386 | 81.5 | 95.3 | 83.5 | 96.2 |
| ViT-B-VTN [63] | IN-21K | 250×1×1 | 3992 | 78.6 | 93.7 | - | - |
| TimeFormer-HR [3] | IN-21K | 16×3×1 | 5109 | 79.7 | 94.4 | 82.4 | 96.0 |
| TimeFormer-L [3] | IN-21K | 96×3×1 | 7140 | 80.7 | 94.7 | 82.2 | 95.5 |
| STAM [71] | IN-21K | 64×1×1 | 1040 | 79.2 | - | - | - |
| X-ViT [5] | IN-21K | 8×3×1 | 425 | 78.5 | 93.7 | 82.5 | 95.4 |
| X-ViT [5] | IN-21K | 16×3×1 | 850 | 80.2 | 94.7 | 84.5 | 96.3 |
| Mformer-HR [64] | IN-21K | 16×3×10 | 28764 | 81.1 | 95.2 | 82.7 | 96.1 |
| MViT-B,16×4 [27] | - | 16×1×5 | 353 | 78.4 | 93.5 | 82.1 | 95.7 |
| MViT-B,32×3 [27] | - | 32×1×5 | 850 | 80.2 | 94.4 | 83.4 | 96.3 |
| ViViT-L [1] | IN-21K | 16×3×4 | 17352 | 80.6 | 94.7 | 82.5 | 95.6 |
| ViViT-L [1] | JFT-300M | 16×3×4 | 17352 | 82.8 | 95.3 | 84.3 | 96.2 |
| ViViT-H [1] | JFT-300M | 16×3×4 | 99792 | 84.8 | 95.8 | 85.8 | 96.5 |
| Swin-T [57] | IN-1K | 32×3×4 | 1056 | 78.8 | 93.6 | - | - |
| Swin-B [57] | IN-1K | 32×3×4 | 3384 | 80.6 | 94.6 | - | - |
| Swin-B [57] | IN-21K | 32×3×4 | 3384 | 82.7 | 95.5 | 84.0 | 96.5 |
| Swin-L-384† [57] | IN-21K | 32×5×10 | 105350 | 84.9 | 96.7 | 86.1 | 97.3 |
| UniFormer-S | IN-1K | 16×1×4 | 167 | 80.8 | 94.7 | 82.8 | 95.8 |
| UniFormer-B | IN-1K | 16×1×4 | 389 | 82.0 | 95.1 | 84.0 | 96.4 |
| UniFormer-B | IN-1K | 32×1×4 | 1036 | 82.9 | 95.4 | 84.8 | 96.7 |
| UniFormer-B | IN-1K | 32×3×4 | 3108 | 83.0 | 95.4 | 84.9 | 96.7 |

TABLE 3. Comparison with the state-of-the-art on Kinetics-400&600. Our UniFormer outperforms most of the current methods with much fewer computation cost.

120 f). The second part lists the recent methods based on vision transformers. With only ImageNet-1K pre-training, UniFormer-B_{16 f} surpasses most existing backbones with large dataset pre-training. For example, compared with ViViT-L [1] pre-trained from JFT-300M [74] and Swin-B [57] pre-trained from ImageNet-21K, UniFormer-B_{32 f} obtains comparable performance (82.9% vs. 82.8% and 82.7%) with **16.7**× and **3.3**× fewer computation on both Kinetics-400 and Kinetics-600. These results demonstrate the efficiency and effectiveness of our UniFormer in the video domain.

5.2.3 Results on Something-Something

Table 4 presents the results on Something-Something V1&V2. Since these datasets require robust temporal relation modeling, it is difficult for the CNN-based methods to capture long-term dependencies, which leads to their worse results. On the contrary, video transformers are good at processing long sequential data and demonstrate better transfer learning capabilities [110], thus they achieve higher accuracy but with large computation cost. In contrast, our UniFormer-S_{16 f} combines the advantages of both convolution and self-attention, obtaining **54.4%/65.0%** in Something-Something V1/V2 with only **42** GFLOPs. It also demonstrates that small models benefit from large dataset pre-training (53.8% vs. 54.4%), but large models do not (59.1% vs. 58.8%). Besides, it is worth noting that our UniFormer pre-trained from Kinetics-600 outperforms all the current methods under the same settings. In fact, our best model achieves the new state-of-the-art results: **61.0%** top-1 accuracy on Something-Something V1 (**4.2%** higher than TDN_{EN}) [87] and **71.2%** top-1 accuracy on Something-Something V2 (**1.6%** higher than Swin-B [57]). Such

| Method | Pretrain | #Frame | FLOPs (G) | SSV1 | | SSV2 | |
|---------------------------|----------|------------|--------------|-------------|-------------|-------------|-------------|
| | | | | Top-1 | Top-5 | Top-1 | Top-5 |
| TSN [86] | IN-1K | 16×1×1 | 66 | 19.9 | 47.3 | 30.0 | 60.5 |
| TSM [54] | IN-1K | 16×1×1 | 66 | 47.2 | 77.1 | - | - |
| GST [62] | IN-1K | 16×1×1 | 59 | 48.6 | 77.9 | 62.6 | 87.9 |
| TEINet [58] | IN-1K | 16×1×1 | 66 | 49.9 | - | 62.1 | - |
| TEA [52] | IN-1K | 16×1×1 | 70 | 51.9 | 80.3 | - | - |
| MSNet [47] | IN-1K | 16×1×1 | 101 | 52.1 | 82.3 | 64.7 | 89.4 |
| CT-Net [49] | IN-1K | 16×1×1 | 75 | 52.5 | 80.9 | 64.5 | 89.3 |
| CT-Net _{EN} [49] | IN-1K | 8+12+16+24 | 280 | 56.6 | 83.9 | 67.8 | 91.1 |
| TDN [87] | IN-1K | 16×1×1 | 72 | 53.9 | 82.1 | 65.3 | 89.5 |
| TDN _{EN} [87] | IN-1K | 8+16 | 198 | 56.8 | 84.1 | 68.2 | 91.6 |
| TimeFormer-HR [3] | IN-21K | 16×3×1 | 5109 | - | - | 62.5 | - |
| TimeFormer-L [3] | IN-21K | 96×3×1 | 7140 | - | - | 62.3 | - |
| X-ViT [5] | IN-21K | 16×3×1 | 850 | - | - | 65.2 | 90.6 |
| X-ViT [5] | IN-21K | 32×3×1 | 1270 | - | - | 65.4 | 90.7 |
| Mformer-HR [64] | K400 | 16×3×1 | 2876 | - | - | 67.1 | 90.6 |
| Mformer-L [64] | K400 | 32×3×1 | 3555 | - | - | 68.1 | 91.2 |
| ViViT-L [1] | K400 | 16×3×4 | 11892 | - | - | 65.4 | 89.8 |
| MViT-B,64×3 [27] | K400 | 64×1×3 | 1365 | - | - | 67.7 | 90.9 |
| MViT-B-24,32×3 [27] | K600 | 32×1×3 | 708 | - | - | 68.7 | 91.5 |
| Swin-B [57] | K400 | 32×3×1 | 963 | - | - | 69.6 | 92.7 |
| UniFormer-S | K400 | 16×1×1 | 42 | 53.8 | 81.9 | 63.5 | 88.5 |
| UniFormer-S | K600 | 16×1×1 | 42 | 54.4 | 81.8 | 65.0 | 89.3 |
| UniFormer-S | K400 | 16×3×1 | 125 | 57.2 | 84.9 | 67.7 | 91.4 |
| UniFormer-S | K600 | 16×3×1 | 125 | 57.6 | 84.9 | 69.4 | 92.1 |
| UniFormer-B | K400 | 16×3×1 | 290 | 59.1 | 86.2 | 70.4 | 92.8 |
| UniFormer-B | K600 | 16×3×1 | 290 | 58.8 | 86.5 | 70.2 | 93.0 |
| UniFormer-B | K400 | 32×3×1 | 777 | 60.9 | 87.3 | 71.2 | 92.8 |
| UniFormer-B | K600 | 32×3×1 | 777 | 61.0 | 87.6 | 71.2 | 92.8 |
| UniFormer-B | K400 | 32×3×2 | 1554 | 61.0 | 87.3 | 71.4 | 92.8 |
| UniFormer-B | K600 | 32×3×2 | 1554 | 61.2 | 87.6 | 71.3 | 92.8 |

TABLE 4. Comparison with the state-of-the-art on Something-Something V1&V2. Our UniFormer achieves new state-of-the-art performances on both datasets.

results verify the high capability of spatiotemporal learning.

5.3 Object Detection and Instance Segmentation

5.3.1 Settings

We benchmark our models on object detection and instance segmentation with COCO2017 [55]. The ImageNet-1K pre-trained models are utilized as backbones and then armed with two representative frameworks: Mask R-CNN [6] and Cascade Mask R-CNN [34]. Our codes are mainly based on mmdetection [13], and the training strategies are the same as Swin Transformer [56]. We adopt two training schedules: 1× schedule with 12 epochs and 3× schedule with 36 epochs. For the 1× schedule, the shorter side of the image is resized to 800 while keeping the longer side no more than 1333. As for the 3× schedule, we apply the multi-scale training strategy to randomly resize the shorter side between 480 to 800. Besides, we use AdamW optimizer with the initial learning rate of 1e-4 and weight decay 0.05. To regularize the training, we set the stochastic depth drop rates to 0.1/0.3 and 0.2/0.4 for our small/base models with Mask R-CNN and Cascade Mask R-CNN.

5.3.2 Results

Table 5 reports box mAP (AP^b) and mask mAP (AP^m) of the Mask R-CNN framework. It shows that our UniFormer variants outperform all the CNN and Transformer backbones. To reduce the training cost for object detection, we utilize a hybrid UniFormer style with a window size of 14 in Stage3 (label by h_{14}). Specifically, with 1× schedule, our UniFormer brings 7.0-7.6 points of box mAP and 6.7-7.2 mask mAP against ResNet [35] at comparable settings. Compared with the popular Swin Transformer [56], our UniFormer achieves 2.6-3.4 points of box mAP and 2.2-

| Method | #Params (M) | FLOPs (G) | Mask R-CNN 1× schedule | | | | | | Mask R-CNN 3× + MS schedule | | | | | |
|----------------------------|----------------|--------------|------------------------|-------------|-------------|-------------|-------------|-------------|-----------------------------|-------------|-------------|-------------|-------------|-------------|
| | | | AP^b | AP_{50}^b | AP_{75}^b | AP^m | AP_{50}^m | AP_{75}^m | AP^b | AP_{50}^b | AP_{75}^b | AP^m | AP_{50}^m | AP_{75}^m |
| Res50 [35] | 44 | 260 | 38.0 | 58.6 | 41.4 | 34.4 | 55.1 | 36.7 | 41.0 | 61.7 | 44.9 | 37.1 | 58.4 | 40.1 |
| PVT-S [89] | 44 | 245 | 40.4 | 62.9 | 43.8 | 37.8 | 60.1 | 40.3 | 43.0 | 65.3 | 46.9 | 39.9 | 62.5 | 42.8 |
| TwinsP-S [15] | 44 | 245 | 42.9 | 65.8 | 47.1 | 40.0 | 62.7 | 42.9 | 46.8 | 69.3 | 51.8 | 42.6 | 66.3 | 46.0 |
| Twins-S [15] | 44 | 228 | 43.4 | 66.0 | 47.3 | 40.3 | 63.2 | 43.4 | 46.8 | 69.2 | 51.2 | 42.6 | 66.3 | 45.8 |
| Swin-T [56] | 48 | 264 | 42.2 | 64.6 | 46.2 | 39.1 | 61.6 | 42.0 | 46.0 | 68.2 | 50.2 | 41.6 | 65.1 | 44.8 |
| ViL-S [107] | 45 | 218 | 44.9 | 67.1 | 49.3 | 41.0 | 64.2 | 44.1 | 47.1 | 68.7 | 51.5 | 42.7 | 65.9 | 46.2 |
| Focal-T [97] | 49 | 291 | 44.8 | 67.7 | 49.2 | 41.0 | 64.7 | 44.2 | 47.2 | 69.4 | 51.9 | 42.7 | 66.5 | 45.9 |
| UniFormer-S _{h14} | 41 | 269 | 45.6 | 68.1 | 49.7 | 41.6 | 64.8 | 45.0 | 48.2 | 70.4 | 52.5 | 43.4 | 67.1 | 47.0 |
| Res101 [35] | 63 | 336 | 40.4 | 61.1 | 44.2 | 36.4 | 57.7 | 38.8 | 42.8 | 63.2 | 47.1 | 38.5 | 60.1 | 41.3 |
| X101-32 [96] | 63 | 340 | 41.9 | 62.5 | 45.9 | 37.5 | 59.4 | 40.2 | 44.0 | 64.4 | 48.0 | 39.2 | 61.4 | 41.9 |
| PVT-M [89] | 64 | 302 | 42.0 | 64.4 | 45.6 | 39.0 | 61.6 | 42.1 | 44.2 | 66.0 | 48.2 | 40.5 | 63.1 | 43.5 |
| TwinsP-B [15] | 64 | 302 | 44.6 | 66.7 | 48.9 | 40.9 | 63.8 | 44.2 | 47.9 | 70.1 | 52.5 | 43.2 | 67.2 | 46.3 |
| Twins-B [15] | 76 | 340 | 45.2 | 67.6 | 49.3 | 41.5 | 64.5 | 44.8 | 48.0 | 69.5 | 52.7 | 43.0 | 66.8 | 46.6 |
| Swin-S [56] | 69 | 354 | 44.8 | 66.6 | 48.9 | 40.9 | 63.4 | 44.2 | 48.5 | 70.2 | 53.5 | 43.3 | 67.3 | 46.6 |
| Focal-S [97] | 71 | 401 | 47.4 | 69.8 | 51.9 | 42.8 | 66.6 | 46.1 | 48.8 | 70.5 | 53.6 | 43.8 | 67.7 | 47.2 |
| CSWin-S [22] | 54 | 342 | 47.9 | 70.1 | 52.6 | 43.2 | 67.1 | 46.2 | 50.0 | 71.3 | 54.7 | 44.5 | 68.4 | 47.7 |
| Swin-B [56] | 107 | 496 | 46.9 | - | - | 42.3 | - | - | 48.5 | 69.8 | 53.2 | 43.4 | 66.8 | 46.9 |
| Focal-B [97] | 110 | 533 | 47.8 | - | - | 43.2 | - | - | 49.0 | 70.1 | 53.6 | 43.7 | 67.6 | 47.0 |
| UniFormer-B _{h14} | 69 | 399 | 47.4 | 69.7 | 52.1 | 43.1 | 66.0 | 46.5 | 50.3 | 72.7 | 55.3 | 44.8 | 69.0 | 48.3 |

TABLE 5. Object detection and instance segmentation with Mask R-CNN on COCO val2017. The FLOPs are measured at resolution 800×1280. All the models are pre-trained on ImageNet-1K [21]. ‘h14’ refers to hybrid UniFormer style with window size of 14 in Stage3.

| Method | #Params (M) | FLOPs (G) | 3× + MS schedule | | | | | |
|----------------------------|----------------|--------------|------------------|-------------|-------------|-------------|-------------|-------------|
| | | | AP^b | AP_{50}^b | AP_{75}^b | AP^m | AP_{50}^m | AP_{75}^m |
| Res50 [35] | 82 | 739 | 46.3 | 64.3 | 50.5 | 40.1 | 61.7 | 43.4 |
| DeiT [78] | 80 | 889 | 48.0 | 67.2 | 51.7 | 41.4 | 64.2 | 44.3 |
| Swin-T [56] | 86 | 745 | 50.5 | 69.3 | 54.9 | 43.7 | 66.6 | 47.1 |
| Shuffle-T [39] | 86 | 746 | 50.8 | 69.6 | 55.1 | 44.1 | 66.9 | 48.0 |
| Focal-T [97] | 87 | 770 | 51.5 | 70.6 | 55.9 | - | - | - |
| UniFormer-S _{h14} | 79 | 747 | 52.1 | 71.1 | 56.6 | 45.2 | 68.3 | 48.9 |
| X101-32 [96] | 101 | 819 | 48.1 | 66.5 | 52.4 | 41.6 | 63.9 | 45.2 |
| Swin-S [56] | 107 | 838 | 51.8 | 70.4 | 56.3 | 44.7 | 67.9 | 48.5 |
| Shuffle-S [39] | 107 | 844 | 51.9 | 70.9 | 56.4 | 44.9 | 67.8 | 48.6 |
| CSWin-S [22] | 92 | 820 | 53.7 | 72.2 | 58.4 | 46.4 | 69.6 | 50.6 |
| Swin-B [56] | 145 | 972 | 51.9 | 70.9 | 57.0 | 45.3 | 68.5 | 48.9 |
| Shuffle-B [39] | 145 | 989 | 52.2 | 71.3 | 57.0 | 45.3 | 68.5 | 48.9 |
| UniFormer-B _{h14} | 107 | 878 | 53.8 | 72.8 | 58.5 | 46.4 | 69.9 | 50.4 |

TABLE 6. Object detection and instance segmentation with Cascade Mask R-CNN on COCO val2017. All the models are trained with 3× multi-scale schedule.

2.5 mask mAP improvement. Moreover, with 3× schedule and multi-scale training, our models still consistently surpass CNN and Transformer counterparts. For example, our UniFormer-B outperforms the powerful CSwin-S [22] by +0.3 box mAP and +0.3 mask mAP, and even better than larger backbones such as Swin-B and Focal-B [97]. Table 6 reports the results with Cascade Mask R-CNN framework. It also shows our UniFormer achieves consistent improvement, demonstrating its stronger context modeling capacity.

5.4 Semantic Segmentation

5.4.1 Settings

Our semantic segmentation experiments are conducted on the ADE20k [109] dataset and our codes are based on mmseg [18]. We adopt the popular Semantic FPN [44] and Upernet [93] as the basic framework. For a fair comparison, we follow the same setting of PVT [89] to train Semantic FPN 80k iterations with cosine learning rate schedule [61]. As for Upernet, we simply apply the settings of Swin Transformer [56] and train the models for 160k iterations. The stochastic depth drop rates are set to 0.1/0.2 and 0.25/0.4 for

| Method | Semantic FPN 80K | | |
|----------------------------|------------------|----------|-------------|
| | #Param(M) | FLOPs(G) | mIoU(%) |
| Res50 [35] | 29 | 183 | 36.7 |
| PVT-S [89] | 28 | 161 | 39.8 |
| TwinsP-S [15] | 28 | 162 | 44.3 |
| Twins-S [15] | 28 | 144 | 43.2 |
| Swin-T [56] | 32 | 182 | 41.5 |
| UniFormer-S _{h32} | 25 | 199 | 46.2 |
| UniFormer-S | 25 | 247 | 46.6 |
| Res101 [35] | 48 | 260 | 38.8 |
| PVT-M [89] | 48 | 219 | 41.6 |
| TwinsP-B [15] | 48 | 220 | 44.9 |
| Twins-B [15] | 60 | 261 | 45.3 |
| Swin-S [56] | 53 | 274 | 45.2 |
| Swin-B [56] | 91 | 422 | 46.0 |
| UniFormer-B _{h32} | 54 | 350 | 47.7 |
| UniFormer-B | 54 | 471 | 48.0 |

TABLE 7. Semantic segmentation with semantic FPN on ADE20K. The FLOPs are measured at resolution 512×2048. ‘h32’ means we utilize hybrid UniFormer blocks with window size of 32 in Stage3.

small/base variants with Semantic FPN and Upernet respectively.

5.4.2 Results

Table 9 reports the results of single and multi-scale testing. It shows that with the Semantic FPN framework, our UniFormer-S_{h32}/B_{h32} achieve +4.7/+2.5 higher mIoU than the Swin Transformer [56] with similar model sizes. When equipped with the UperNet framework, they achieve +2.5/+1.9 mIoU and +2.7/+1.2 MS mIoU improvement. Furthermore, when utilizing the global MHRA, the results are consistently improved but with a large computation cost. More results can be found in Table 16.

5.5 Pose Estimation

5.5.1 Settings

We evaluate the performance of UniFormer on the COCO2017 [55] human pose estimation benchmark. For a fair comparison with previous SOTA methods, we employ a single Top-Down head after

| Arch. | Method | Input Size | #Param(M) | FLOPs(G) | AP | AP ⁵⁰ | AP ⁷⁵ | AP ^M | AP ^L | AR |
|-----------|--------------------------|------------|-----------|----------|-------------|------------------|------------------|-----------------|-----------------|-------------|
| CNN | SimpleBaseline-R101 [92] | 256×192 | 53.0 | 12.4 | 71.4 | 89.3 | 79.3 | 68.1 | 78.1 | 77.1 |
| | SimpleBaseline-R152 [92] | 256×192 | 68.6 | 15.7 | 72.0 | 89.3 | 79.8 | 68.7 | 78.9 | 77.8 |
| | HRNet-W32 [85] | 256×192 | 28.5 | 7.1 | 74.4 | 90.5 | 81.9 | 70.8 | 81.0 | 78.9 |
| | HRNet-W48 [85] | 256×192 | 63.6 | 14.6 | 75.1 | 90.6 | 82.2 | 71.5 | 81.8 | 80.4 |
| CNN+Trans | TransPose-H-A6 [98] | 256×192 | 17.5 | 21.8 | 75.8 | - | - | - | - | 80.8 |
| | TokenPose-L/D24 [51] | 256×192 | 27.5 | 11.0 | 75.8 | 90.3 | 82.5 | 72.3 | 82.7 | 80.9 |
| | HRFormer-S [102] | 256×192 | 7.8 | 3.3 | 74.0 | 90.2 | 81.2 | 70.4 | 80.7 | 79.4 |
| | HRFormer-B [102] | 256×192 | 43.2 | 14.1 | 75.6 | 90.8 | 82.8 | 71.7 | 82.6 | 80.8 |
| | UniFormer-S | 256×192 | 25.2 | 4.7 | 74.0 | 90.3 | 82.2 | 66.8 | 76.7 | 79.5 |
| | UniFormer-B | 256×192 | 53.5 | 9.2 | 75.0 | 90.6 | 83.0 | 67.8 | 77.7 | 80.4 |
| CNN | SimpleBaseline-R152 [92] | 384×288 | 68.6 | 35.6 | 74.3 | 89.6 | 81.1 | 70.5 | 79.7 | 79.7 |
| | HRNet-W32 [85] | 384×288 | 28.5 | 16.0 | 75.8 | 90.6 | 82.7 | 71.9 | 82.8 | 81.0 |
| | HRNet-W48 [85] | 384×288 | 63.6 | 32.9 | 76.3 | 90.8 | 82.9 | 72.3 | 83.4 | 81.2 |
| CNN+Trans | PRTR [48] | 384×288 | 57.2 | 21.6 | 73.1 | 89.4 | 79.8 | 68.8 | 80.4 | 79.8 |
| | PRTR [48] | 512×384 | 57.2 | 37.8 | 73.3 | 89.2 | 79.9 | 69.0 | 80.9 | 80.2 |
| | HRFormer-S [102] | 384×288 | 7.8 | 7.2 | 75.6 | 90.3 | 82.2 | 71.6 | 82.5 | 80.7 |
| | HRFormer-B [102] | 384×288 | 43.2 | 30.7 | 77.2 | 91.0 | 83.6 | 73.2 | 84.2 | 82.0 |
| | UniFormer-S | 384×288 | 25.2 | 11.1 | 75.9 | 90.6 | 83.4 | 68.6 | 79.0 | 81.4 |
| | UniFormer-B | 384×288 | 53.5 | 22.1 | 76.7 | 90.8 | 84.0 | 69.3 | 79.7 | 81.9 |
| | UniFormer-S | 448×320 | 25.2 | 14.8 | 76.2 | 90.6 | 83.2 | 68.6 | 79.4 | 81.4 |
| | UniFormer-B | 448×320 | 53.5 | 29.6 | 77.4 | 91.1 | 84.4 | 70.2 | 80.6 | 82.5 |

TABLE 8. Human Pose estimation on COCO pose estimation val set. All the models are pre-trained on ImageNet-1K [21].

| Method | Upernet 160K | | | |
|----------------------------|--------------|----------|-------------|-------------|
| | #Param.(M) | FLOPs(G) | mIoU(%) MS | mIoU(%) |
| TwinsP-S [15] | 55 | 919 | 46.2 | 47.5 |
| Twins-S [15] | 54 | 901 | 46.2 | 47.1 |
| Swin-T [56] | 60 | 945 | 44.5 | 45.8 |
| Focal-T [97] | 62 | 998 | 45.8 | 47.0 |
| Shuffle-T [39] | 60 | 949 | 46.6 | 47.8 |
| UniFormer-S _{h32} | 52 | 955 | 47.0 | 48.5 |
| UniFormer-S | 52 | 1008 | 47.6 | 48.5 |
| Res101 [35] | 86 | 1029 | - | 44.9 |
| TwinsP-B [15] | 74 | 977 | 47.1 | 48.4 |
| Twins-B [15] | 89 | 1020 | 47.7 | 48.9 |
| Swin-S [56] | 81 | 1038 | 47.6 | 49.5 |
| Focal-T [97] | 85 | 1130 | 48.0 | 50.0 |
| Shuffle-S [39] | 81 | 1044 | 48.4 | 49.6 |
| Swin-B [56] | 121 | 1188 | 48.1 | 49.7 |
| Focal-B [97] | 126 | 1354 | 49.0 | 50.5 |
| Shuffle-B [39] | 121 | 1196 | 49.0 | 50.5 |
| UniFormer-B _{h32} | 80 | 1106 | 49.5 | 50.7 |
| UniFormer-B | 80 | 1227 | 50.0 | 50.8 |

TABLE 9. Semantic segmentation with Upernet on ADE20K. The FLOPs are measured at resolution 512×2048. ‘h32’ means we utilize hybrid UniFormer blocks with window size of 32 in Stage3.

our backbones. We follow the same training and evaluation setting of mmpose [17] as HRFormer [102]. In addition, the batch size and stochastic depth drop rates are set to 1024/256 and 0.2/0.5 for small/base variants during training.

5.5.2 Results

Table 8 reports results of different input resolutions on COCO validation set. Compared with previous SOTA CNN models, our UniFormer-B surpasses HRNet-W48 [85] by 0.4% AP with fewer parameters (53.5M vs. 63.6M) and FLOPs (22.1G vs. 32.9G). Moreover, our UniFormer-B can outperform the current best approach HRFormer [102] by 0.2% AP with smaller FLOPs (29.6G vs. 30.7G). It is worth noting that HRFormer [102], PRTR [48], TokenPose [51] and TransPose [98] are sophisticatedly designed for pose estimation task. On the contrary, our UniFormer can

outperform all of them as a simple yet effective backbone.

5.6 Ablation Studies

To inspect the effectiveness of UniFormer as the backbone, we ablate each key structure design and evaluate the performance on image and video classification datasets. Furthermore, for video backbones, we explore the vital designs of pre-training, training and testing. Finally, we demonstrate the efficiency of our adaption on detection, segmentation and pose estimation.

5.6.1 Model designs for image and video backbones

In this section, we conduct ablation studies of the vital components as shown in Table 10. All video models are trained with 16 frames.

FFN. As mentioned in Section 3.2, our UniFormer blocks in the shallow layers are instantiated as a transformer-style MobileNet block [81] with extra FFN as in ViT [23]. Hence, we first investigate its effectiveness by replacing our UniFormer blocks in the shallow layers with MobileNet blocks [69]. BN and GELU are added as the original paper, but the expand ratios are set to 3 for similar parameters. Note that the dynamic position embedding is kept for a fair comparison. As expected, our UniFormer outperforms such MobileNet block both in ImageNet (+0.3%) and Kinetics-400 (+0.7%). It shows that, FFN in our model can further mix token context at each position to boost classification accuracy.

DPE. With dynamic position embedding, our UniFormer obviously improve the top-1 accuracy by +0.5% on ImageNet, but +1.7% on Kinetics-400. It shows that via encoding the position information, our DPE can maintain spatial and temporal order, thus contributing to better representation learning, especially for video.

MHRA. In our local token affinity (Eq. 6), we aggregate the context from a small local tube. Hence, we investigate the influence of this tube by changing the size from 3 to 9. Results show that our network is robust to the tube size on both ImageNet and Kinetics-400. We simply choose the kernel size of 5 for better accuracy. More importantly, we investigate the configuration of local and global UniFormer block stage by stage, in order to verify the effectiveness of our network. As shown in row1, 7-10 in Table 10, when we only use local MHRA (LLLL), the computation

| FFN | DPE | MHRA | | ImageNet | | K400 | |
|-----|-----|------|------|----------|-------------|--------|-------------|
| | | Size | Type | #Param | Top-1 | GFLOPs | Top-1 |
| ✓ | ✓ | 5 | LLGG | 21.5 | 82.9 | 41.8 | 79.3 |
| ✗ | ✓ | 5 | LLGG | 21.3 | 82.6 | 41.0 | 78.6 |
| ✓ | ✗ | 5 | LLGG | 21.5 | 82.4 | 41.4 | 77.6 |
| ✓ | ✓ | 3 | LLGG | 21.5 | 82.8 | 41.0 | 79.0 |
| ✓ | ✓ | 7 | LLGG | 21.6 | 82.9 | 43.5 | 79.1 |
| ✓ | ✓ | 9 | LLGG | 21.6 | 82.8 | 46.6 | 78.9 |
| ✓ | ✓ | 5 | LLLL | 23.3 | 81.9 | 31.6 | 77.2 |
| ✓ | ✓ | 5 | LLLG | 22.2 | 82.5 | 31.6 | 78.4 |
| ✓ | ✓ | 5 | LGGG | 21.6 | 82.7 | 39.0 | 79.0 |
| ✓ | ✓ | 5 | GGGG | 20.1 | 82.1 | 72.0 | 75.3 |

TABLE 10. Structure designs. All models are trained for 50 epochs on Kinetics-400 with 16 frames. To guarantee the parameters and computation of all the models are similar, when modifying the stage types, we modify the stage numbers and reduce the computation of self-attention as MViT [27] for LGGG and GGGG.

| Type | Joint | GFLOPs | Pretrain | | SSV1 | |
|------|-------|--------|----------|-------|------------|------------|
| | | | Dataset | Top-1 | Top-1 | Top-5 |
| LLLL | ✓ | 26.1 | IN-1K | 81.0 | 49.2 | 77.4 |
| | | | K400 | 77.4 | 49.2(+0.0) | 77.6(+0.2) |
| LLGG | ✗ | 36.8 | IN-1K | 82.9 | 51.9 | 80.1 |
| | | | K400 | 80.1 | 51.8(-0.1) | 80.1(+0.0) |
| LLGG | ✓ | 41.8 | IN-1K | 82.9 | 52.0 | 80.2 |
| | | | K400 | 80.8 | 53.8(+1.8) | 81.9(+1.7) |

TABLE 11. Transfer learning. Jointly manner performs better.

cost is light. However, the accuracy is largely dropped (-1.0% and -2.1% on ImageNet and Kinetics-400) due to the lack of capacity for learning long-term dependency. When we gradually replace local MHRA with global MHRA, the accuracy becomes better as expected. Unfortunately, the accuracy is dramatically dropped with a heavy computation load when all the layers apply global MHRA (GGGG), i.e., -4.0% on Kinetics-400. It is mainly because that, without local MHRA, the network lacks the ability to extract detailed representations, leading to severe model overfitting with redundant attention for sequential video data. Based on the above results, we choose local MHRA and global MHRA in the first two stages and the last two stages respectively, in order to achieve a preferable computation-accuracy balance.

5.6.2 Pre-training, training and testing for video backbone

In this section, we explore more designs for our video backbones. Firstly, to load 2D pre-trained backbones, it is essential to determine how to inherit self-attention and inflate convolution filters. Hence, we compare the transfer learning performance of different MHRA configurations and inflating methods of filters. Besides, since we use dense sampling [90] for Kinetics, we should confirm the appropriate sampling stride. Furthermore, as we utilize Kinetics pre-trained models for Something-Something, it is interesting to explore the effect of sampling methods and dataset scales for pre-trained models. Finally, we conduct experiments on the testing strategies for different datasets.

Transfer learning. Table 11 presents the results of transfer learning. All models share the same stage numbers but the stage types are different. For Kinetics-400, it clearly shows that the joint version is more powerful than the separate one, verifying that joint spatiotemporal attention can learn more discriminative video representations. As for Something-Something V1, when the

| Dataset | Pretrain | #Frame | 2D | | 3D | |
|---------|----------|--------|-------------|-------------|-------------|-------------|
| | | | Top-1 | Top-5 | Top-1 | Top-5 |
| K400 | IN-1K | 8×1×1 | 74.7 | 90.8 | 74.9 | 90.7 |
| | | 8×1×4 | 78.5 | 93.2 | 78.4 | 93.3 |
| SSV1 | IN-1K | 8×1×1 | 47.9 | 75.8 | 48.3 | 76.1 |
| | | 8×3×1 | 51.4 | 79.6 | 51.3 | 79.7 |
| | K400 | 8×1×1 | 47.9 | 75.6 | 48.6 | 75.6 |
| | | 8×3×1 | 51.3 | 79.4 | 51.5 | 79.5 |

TABLE 12. Inflating methods of filters. Inflating to 3D is better.

| Model | #Frame | FLOPs (G) | Sampling Stride | K400 | | K600 | |
|-------|--------|-----------|-----------------|-------------|-------------|-------------|-------------|
| | | | | Top-1 | Top-5 | Top-1 | Top-5 |
| Small | 16×1×1 | 41.8 | 4 | 76.2 | 92.2 | 79.0 | 93.6 |
| | | | 8 | 78.4 | 92.9 | 80.8 | 94.7 |
| | 16×1×4 | 167.2 | 4 | 80.8 | 94.7 | 82.8 | 95.8 |
| | | | 8 | 80.8 | 94.4 | 82.7 | 95.7 |
| Base | 16×1×1 | 96.7 | 4 | 78.1 | 92.8 | 80.3 | 94.5 |
| | | | 8 | 79.3 | 93.4 | 81.7 | 95.0 |
| | 16×1×4 | 386.8 | 4 | 82.0 | 95.1 | 84.0 | 96.4 |
| | | | 8 | 81.7 | 94.8 | 83.4 | 96.0 |
| Small | 32×1×1 | 109.6 | 2 | 77.3 | 92.4 | - | - |
| | | | 4 | 79.8 | 93.4 | - | - |
| | 32×1×4 | 438.4 | 2 | 81.2 | 94.7 | - | - |
| | | | 4 | 82.0 | 95.1 | - | - |

TABLE 13. Sampling stride of dense sampling. Sparser sampling method often achieves a higher single-clip result.

model is gradually pre-trained from ImageNet to Kinetics-400, the performance of our joint version becomes better. Compared with pre-training from ImageNet, pre-training from Kinetics-400 will further improve the top-1 accuracy by +1.8%. However, such distinct characteristic is not observed in the pure local MHRA structure (LLLL) and UniFormer with divided spatiotemporal attention. It demonstrates that the joint learning manner is preferable for transfer learning, thus we adopt it by default.

Inflating methods. As indicated in I3D [11], we can inflate the 2D convolutional filters for easier optimization. Here we consider whether or not to inflate the filters. Note that the first convolutional filter in the patch stem is always inflated for temporal downsampling. As shown in Table 12, inflating the filters to 3D achieves similar results on Kinetics-400, but obtains obvious performance improvement on Something-Something V1, especially with strong pre-training. We argue that Kinetics-400 is a scene-related dataset, thus 2D convolution is enough to recognize the action. In contrast, Something-Something V1 is a temporal-related dataset, which requires powerful spatiotemporal modeling. Hence, we inflate all the convolutional filters to 3D for better generality.

Sampling stride. For dense sampling strategy, the basic hyperparameter is the frame stride. Intuitively, a larger frame stride will cover a longer frame range, which is essential for better video understanding. In Table 13, we show more results on Kinetics under different sampling methods. As expected, sparser sampling methods (16×8 and 32×4) often achieve higher single-clip results. However, when testing with multi clips, sampling with a frame stride of 4 always performs better.

Sampling methods of Kinetics pre-trained model. For Something-Something, we uniformly sample input frames as input. Since we load Kinetics pre-trained models for fast convergence, it is necessary to find out whether pre-trained models that cover more frames can help fine-tuning. Table 14 shows that, though sparse sampling and inputting more frames help pre-training (Table

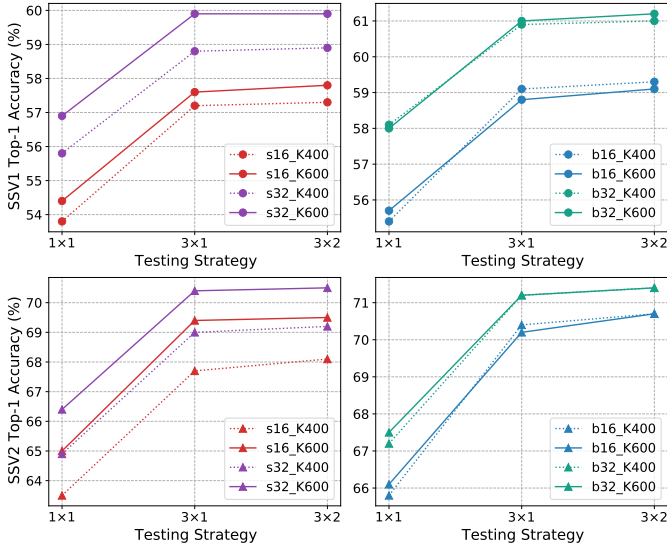


Fig. 6. Pre-trained dataset scales. Small models are eager for larger dataset pre-training on both Something-Something V1 and V2.

| Model | Input Frame | Pre-trained Sampling | Single-clip | | Multi-crop | |
|-------|-------------|----------------------|-------------|-------------|-------------|-------------|
| | | | Top-1 | Top-5 | Top-1 | Top-5 |
| Small | 16 | 16×4 | 53.8 | 81.9 | 57.2 | 84.9 |
| | | 16×8 | 53.7 | 81.3 | 57.3 | 84.6 |
| Base | 16 | 16×4 | 55.4 | 82.9 | 59.1 | 86.2 |
| | | 16×8 | 55.5 | 83.1 | 58.8 | 86.2 |
| Small | 32 | 16×4 | 55.8 | 83.6 | 58.8 | 86.4 |
| | | 32×2 | 55.6 | 83.1 | 58.6 | 85.6 |
| | | 32×4 | 55.9 | 82.9 | 58.9 | 86.0 |

TABLE 14. Sampling methods of Kinetics pre-trained model. All models are pre-trained on K400 and fine-tuned on Sth-Sth V1.

13), different pre-trained models achieve similar performances for fine-tuning. We apply 16×4 pre-training for better generalization.

Pre-trained dataset scales. In Figure 6, we show more results on Something-Something with Kinetics-400/600 pre-training. For UniFormer-S, Kinetics-600 pre-training consistently performs better than Kinetics-400 pre-training, especially for large benchmark Something-Something V2. However, both of them achieve comparable results for UniFormer-B. These results indicate that small models are harder to converge and eager for larger dataset pre-training, but big models are not.

Testing strategies. We evaluate our network with various numbers of clips and crops for the validation videos on different datasets. As shown in Figure 7, since Kinetics is a scene-related dataset and trained with dense sampling, multi-clip testing is preferable to cover more frames for boosting performance. Alternatively, Something-Something is a temporal-related dataset and trained with uniform sampling, so multi-crop testing is better for capturing the discriminative motion for boosting performance.

5.6.3 Adaption designs for downstream tasks

We verify the effectiveness of our adaption for dense prediction tasks in Table 15, Table 16 and Table 17. ‘W’, ‘H’ and ‘G’ refer to window, hybrid and global UniFormer style in Stage3 respectively. Note that the pre-trained global UniFormer block can be seen as a window UniFormer block with large window size, thus the minimal window size in our experiments is 224/32=14.

Table 15 shows results on object detection. Though the hybrid style performs worse than the global style with the 1× schedule, it

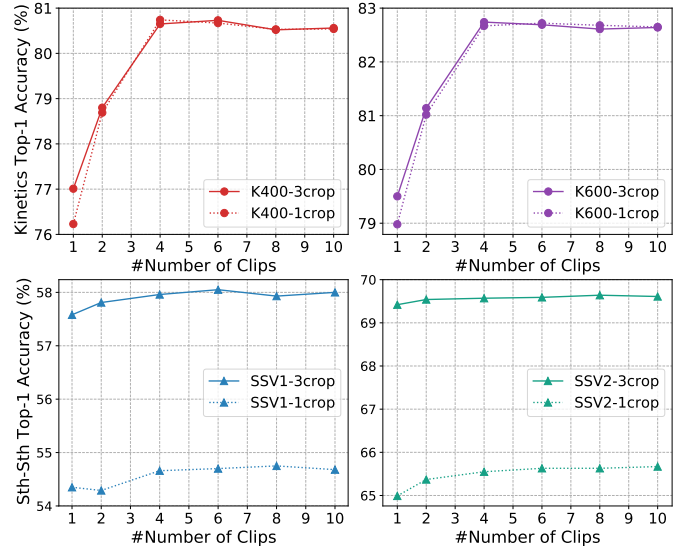


Fig. 7. Multi-clip/crop testing strategies. Multi-clip testing is better for Kinetics and multi-crop testing is better for Something-Something.

| Type | FLOPs (G) | 1× + MS | | | | 3× + MS | | | |
|------|-----------|-------------|-------------|-------------|-------------|-------------|-------------|-------------|-------------|
| | | AP^b | AP_{50}^b | AP^m | AP_{50}^m | AP^b | AP_{50}^b | AP^m | AP_{50}^m |
| W-14 | 250 | 45.0 | 67.8 | 40.8 | 64.7 | 47.5 | 69.8 | 43.0 | 66.7 |
| H-14 | 269 | 45.4 | 68.2 | 41.4 | 64.9 | 48.2 | 70.4 | 43.4 | 67.1 |
| G | 326 | 45.8 | 68.7 | 41.5 | 50.5 | 48.1 | 70.1 | 43.4 | 67.1 |

TABLE 15. Adaption types for object detection.

achieves comparable results with the 3× schedule, which indicates that training enough epochs can narrow the performance gap. We further conduct experiments on semantic segmentation with different model variants in Table 16. As expected, large window size and global UniFormer blocks contribute to better performances, especially for big models. Moreover, when testing with multi-scale inputs, hybrid style with a window size of 32 obtains similar results to the global style. As for human pose estimation (Table 17), due to the small input resolution, i.e. 384×288, utilizing window style requires more computation for zero paddings. We simply apply global UniFormer blocks for better computation-accuracy balance.

5.7 Visualizations

In Figure 8, We apply Grad-CAM [70] to show the areas of the greatest concern in the last layer. Images are sampled from ImageNet validation set [21] and the video is sampled from Kinetics-400 validation set [10]. It reveals that GGGG struggles to focus on the key object, i.e., the mountain and the skateboard, as it blindly compares the similarity of all tokens in all layers. Alternatively, LLLL only performs local aggregation. Hence, its attention tends to be coarse and inaccurate without a global view. Different from both cases, our UniFormer with LLGG can cooperatively learn local and global contexts in a joint manner. As a result, it can effectively capture the most discriminative information, by paying precise attention to the mountain and the skateboard.

In Figure 9, we further conduct visualization on validation datasets for various downstream tasks. Such robust qualitative results demonstrate the effectiveness of our UniFormer backbones.

6 CONCLUSION

In this paper, we propose a novel UniFormer for efficient visual recognition, which can effectively unify convolution and self-attention in a concise transformer format to overcome redundancy and dependency. We adopt local MHRA in shallow layers to largely

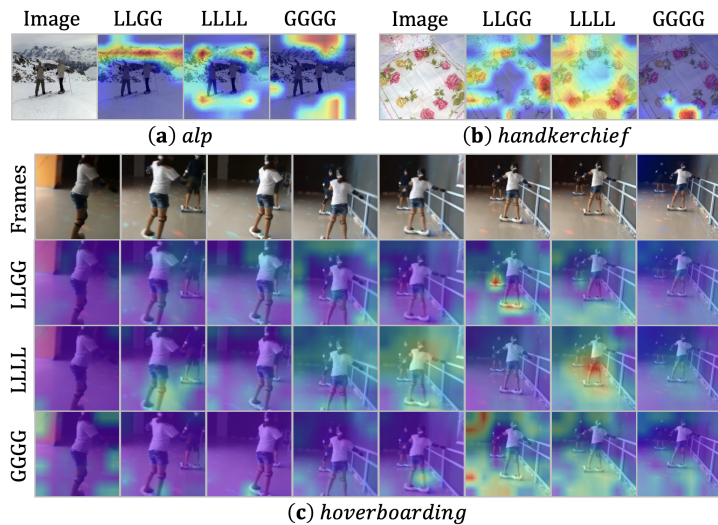


Fig. 8. Attention visualization of different structures.

| Model | Type | Semantic FPN | | UperNet | |
|-------|------|--------------|-------------|-------------|---------------------|
| | | GFLOPs | mIoU(%) | GFLOPs (MS) | mIoU(%) |
| Small | H-14 | 190 | 46.3 | 947 | 46.9(48.0) |
| | W-32 | 183 | 45.2 | 939 | 46.6(48.4) |
| | H-32 | 199 | 46.2 | 955 | 47.0(48.5) |
| | G | 247 | 46.6 | 1004 | 47.6(48.5) |
| Base | H-14 | 328 | 47.0 | 1085 | 48.9(50.0) |
| | W-32 | 310 | 47.2 | 1066 | 49.1(50.6) |
| | H-32 | 350 | 47.7 | 1106 | 49.5(50.7) |
| | G | 471 | 48.0 | 1227 | 50.0(50.8) |

TABLE 16. Adaption types for semantic segmentation.

| Type | Input Size | FLOPs (G) | AP | AP^{50} | AP^{75} | AP^M | AP^L | AR |
|------|------------|-----------|-------------|-----------|-------------|-------------|-------------|-------------|
| W-14 | 384×288 | 12.3 | 76.1 | 90.8 | 83.2 | 68.9 | 79.1 | 81.1 |
| H-14 | 384×288 | 12.0 | 75.9 | 90.7 | 83.2 | 68.6 | 78.9 | 81.0 |
| G | 384×288 | 11.1 | 75.9 | 90.6 | 83.4 | 68.6 | 79.0 | 81.4 |

TABLE 17. Adaption types for pose estimation. Due to zero padding, the models with window UniFormer style require more computation.

reduce computation burden and global MHRA in deep layers to learn global token relation. Extensive experiments demonstrate the powerful modeling capacity of our UniFormer. Via simple yet effective adaption, our UniFormer achieves state-of-the-art results on a broad range of vision tasks with less training cost.

REFERENCES

- [1] A. Arnab, M. Dehghani, G. Heigold, Chen Sun, Mario Lucic, and C. Schmid. Vivit: A video vision transformer. *ArXiv*, abs/2103.15691, 2021. 1, 3, 4, 5, 8
- [2] Jimmy Ba, Jamie Ryan Kiros, and Geoffrey E. Hinton. Layer normalization. *ArXiv*, abs/1607.06450, 2016. 5
- [3] Gedas Bertasius, Heng Wang, and L. Torresani. Is space-time attention all you need for video understanding? *ArXiv*, abs/2102.05095, 2021. 1, 2, 3, 4, 5, 8
- [4] Andrew Brock, Soham De, Samuel L. Smith, and K. Simonyan. High-performance large-scale image recognition without normalization. *ArXiv*, abs/2102.06171, 2021. 7
- [5] Adrian Bulat, Juan-Manuel Pérez-Rúa, Swathikiran Sudhakaran, Brais Martínez, and Georgios Tzimiropoulos. Space-time mixing attention for video transformer. *ArXiv*, abs/2106.05968, 2021. 3, 8
- [6] Zhaowei Cai and Nuno Vasconcelos. Cascade r-cnn: High quality object detection and instance segmentation. *IEEE Transactions on Pattern Analysis and Machine Intelligence*, 2019. 8
- [7] Jie Cao, Yawei Li, K. Zhang, and Luc Van Gool. Video super-resolution transformer. *ArXiv*, abs/2106.06847, 2021. 3

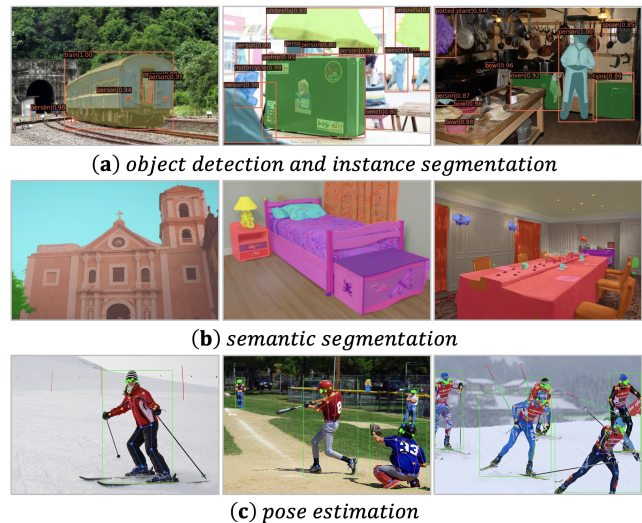


Fig. 9. Qualitative examples for different downstream tasks.

- [8] Nicolas Carion, Francisco Massa, Gabriel Synnaeve, Nicolas Usunier, Alexander Kirillov, and Sergey Zagoruyko. End-to-end object detection with transformers. *ArXiv*, abs/2005.12872, 2020. 3
- [9] João Carreira, Eric Noland, Andras Banki-Horvath, Chloe Hillier, and Andrew Zisserman. A short note about kinetics-600. *ArXiv*, abs/1808.01340, 2018. 6, 7
- [10] João Carreira and Andrew Zisserman. Quo vadis, action recognition? a new model and the kinetics dataset. *2017 IEEE Conference on Computer Vision and Pattern Recognition (CVPR)*, pages 4724–4733, 2017. 6, 7, 12
- [11] João Carreira and Andrew Zisserman. Quo vadis, action recognition? a new model and the kinetics dataset. *2017 IEEE Conference on Computer Vision and Pattern Recognition (CVPR)*, pages 4724–4733, 2017. 3, 5, 7, 11
- [12] Hanting Chen, Yunhe Wang, Tianyu Guo, Chang Xu, Yiping Deng, Zhenhua Liu, Siwei Ma, Chunjing Xu, Chao Xu, and Wen Gao. Pre-trained image processing transformer. *2021 IEEE/CVF Conference on Computer Vision and Pattern Recognition (CVPR)*, pages 12294–12305, 2021. 3
- [13] Kai Chen, Jiaqi Wang, Jiangmiao Pang, Yuhang Cao, Yu Xiong, Xiaoxiao Li, Shuyang Sun, Wansen Feng, Ziwei Liu, Jiarui Xu, Zheng Zhang, Dazhi Cheng, Chenchen Zhu, Tianheng Cheng, Qijie Zhao, Buyu Li, Xin Lu, Rui Zhu, Yue Wu, Jifeng Dai, Jingdong Wang, Jianping Shi, Wanli Ouyang, Chen Change Loy, and Dahua Lin. MMDetection: Open mmlab detection toolbox and benchmark. *arXiv preprint arXiv:1906.07155*, 2019. 8
- [14] Bowen Cheng, Alexander G. Schwing, and Alexander Kirillov. Per-pixel classification is not all you need for semantic segmentation. *ArXiv*, abs/2107.06278, 2021. 3
- [15] Xiangxiang Chu, Zhi Tian, Yuqing Wang, Bo Zhang, Haibing Ren, Xiaolin Wei, Huaxia Xia, and Chunhua Shen. Twins: Revisiting the design of spatial attention in vision transformers. 2021. 5, 9, 10
- [16] Xiangxiang Chu, Bo Zhang, Zhi Tian, Xiaolin Wei, and Huaxia Xia. Do we really need explicit position encodings for vision transformers? *ArXiv*, abs/2102.10882, 2021. 3, 5
- [17] MMPose Contributors. Openmmlab pose estimation toolbox and benchmark. <https://github.com/open-mmlab/mmpose>, 2020. 10
- [18] MMSegmentation Contributors. MMSegmentation: Openmmlab semantic segmentation toolbox and benchmark. <https://github.com/open-mmlab/mms Segmentation>, 2020. 9
- [19] Jean-Baptiste Cordonnier, Andreas Loukas, and Martin Jaggi. On the relationship between self-attention and convolutional layers. *ArXiv*, abs/1911.03584, 2020. 3
- [20] Zihang Dai, Hanxiao Liu, Quoc V. Le, and Mingxing Tan. Coatnet: Marrying convolution and attention for all data sizes. *ArXiv*, abs/2106.04803, 2021. 3, 7
- [21] Jia Deng, Wei Dong, Richard Socher, Li-Jia Li, Kai Li, and Li Fei-Fei. Imagenet: A large-scale hierarchical image database. In *2009 IEEE conference on computer vision and pattern recognition*, pages 248–255. Ieee, 2009. 3, 6, 9, 10, 12
- [22] Xiaoyi Dong, Jianmin Bao, Dongdong Chen, Weiming Zhang, Nenghai Yu, Lu Yuan, Dong Chen, and B. Guo. Cswin transformer: A general

- vision transformer backbone with cross-shaped windows. *ArXiv*, abs/2107.00652, 2021. 3, 5, 6, 7, 9
- [23] A. Dosovitskiy, L. Beyer, Alexander Kolesnikov, Dirk Weissenborn, Xiaohua Zhai, Thomas Unterthiner, M. Dehghani, Matthias Minderer, G. Heigold, S. Gelly, Jakob Uszkoreit, and N. Houlsby. An image is worth 16x16 words: Transformers for image recognition at scale. *ArXiv*, abs/2010.11929, 2021. 1, 4, 5, 10
- [24] Brendan Duke, Abdalla Ahmed, Christian Wolf, Parham Aarabi, and Graham W. Taylor. Sstvos: Sparse spatiotemporal transformers for video object segmentation. *2021 IEEE/CVF Conference on Computer Vision and Pattern Recognition (CVPR)*, pages 5908–5917, 2021. 3
- [25] Maksim Dzabraev, Maksim Kalashnikov, Stepan Alekseevich Komkov, and Aleksandr Petiushko. Mdmmt: Multidomain multimodal transformer for video retrieval. *2021 IEEE/CVF Conference on Computer Vision and Pattern Recognition Workshops (CVPRW)*, pages 3349–3358, 2021. 3
- [26] Haoqi Fan, Yanghao Li, Bo Xiong, Wan-Yen Lo, and Christoph Feichtenhofer. Pyslowfast. <https://github.com/facebookresearch/slowfast>, 2020. 7
- [27] Haoqi Fan, Bo Xiong, Karttikeya Mangalam, Yanghao Li, Zhicheng Yan, J. Malik, and Christoph Feichtenhofer. Multiscale vision transformers. *ArXiv*, abs/2104.11227, 2021. 1, 3, 7, 8, 11
- [28] Christoph Feichtenhofer. X3d: Expanding architectures for efficient video recognition. *2020 IEEE/CVF Conference on Computer Vision and Pattern Recognition (CVPR)*, pages 200–210, 2020. 3, 4, 8
- [29] Christoph Feichtenhofer, Haoqi Fan, Jitendra Malik, and Kaiming He. Slowfast networks for video recognition. *2019 IEEE/CVF International Conference on Computer Vision (ICCV)*, pages 6201–6210, 2019. 1, 3, 7, 8
- [30] Valentin Gabeur, Chen Sun, Alahari Karteek, and Cordelia Schmid. Multi-modal transformer for video retrieval. In *ECCV*, 2020. 3
- [31] Peng Gao, Jiaseen Lu, Hongsheng Li, R. Mottaghi, and Aniruddha Kembhavi. Container: Context aggregation network. *ArXiv*, abs/2106.01401, 2021. 7
- [32] Priya Goyal, Piotr Dollár, Ross B. Girshick, Pieter Noordhuis, Lukasz Wesolowski, Aapo Kyrola, Andrew Tulloch, Yangqing Jia, and Kaiming He. Accurate, large minibatch sgd: Training imagenet in 1 hour. *ArXiv*, abs/1706.02677, 2017. 6, 7
- [33] Raghav Goyal, Samira Ebrahimi Kahou, Vincent Michalski, Joanna Materzynska, Susanne Westphal, Heuna Kim, Valentin Haenel, Ingo Fründ, Peter Yánilos, Moritz Mueller-Freitag, Florian Hoppe, Christian Thraur, Ingo Bax, and Roland Memisevic. The “something something” video database for learning and evaluating visual common sense. *2017 IEEE International Conference on Computer Vision (ICCV)*, pages 5843–5851, 2017. 6, 7
- [34] Kaiming He, Georgia Gkioxari, Piotr Dollár, and Ross Girshick. Mask r-cnn. In *Proceedings of the IEEE international conference on computer vision*, pages 2961–2969, 2017. 8
- [35] Kaiming He, X. Zhang, Shaoqing Ren, and Jian Sun. Deep residual learning for image recognition. *2016 IEEE Conference on Computer Vision and Pattern Recognition (CVPR)*, pages 770–778, 2016. 1, 3, 5, 8, 9, 10
- [36] Shuting He, Haowen Luo, Pichao Wang, F. Wang, Hao Li, and Wei Jiang. Transreid: Transformer-based object re-identification. *ArXiv*, abs/2102.04378, 2021. 3
- [37] Andrew G. Howard, Menglong Zhu, Bo Chen, Dmitry Kalenichenko, Weijun Wang, Tobias Weyand, M. Andreetto, and Hartwig Adam. Mobilenets: Efficient convolutional neural networks for mobile vision applications. *ArXiv*, abs/1704.04861, 2017. 1, 3
- [38] Gao Huang, Zhuang Liu, and Kilian Q. Weinberger. Densely connected convolutional networks. *2017 IEEE Conference on Computer Vision and Pattern Recognition (CVPR)*, pages 2261–2269, 2017. 3
- [39] Zilong Huang, Youcheng Ben, Guozhong Luo, Pei Cheng, Gang Yu, and Bin Fu. Shuffle transformer: Rethinking spatial shuffle for vision transformer. *ArXiv*, abs/2106.03650, 2021. 9, 10
- [40] Sergey Ioffe and Christian Szegedy. Batch normalization: Accelerating deep network training by reducing internal covariate shift. *ArXiv*, abs/1502.03167, 2015. 5
- [41] Boyuan Jiang, Mengmeng Wang, Weihao Gan, Wei Wu, and Junjie Yan. Stm: Spatiotemporal and motion encoding for action recognition. *2019 IEEE International Conference on Computer Vision (ICCV)*, pages 2000–2009, 2019. 3
- [42] Zihang Jiang, Qibin Hou, Li Yuan, Daquan Zhou, Yujun Shi, Xiaojie Jin, Anran Wang, and Jiashi Feng. All tokens matter: Token labeling for training better vision transformers. 2021. 5, 6, 7
- [43] Youngsaeng Jin, David K. Han, and Hanseok Ko. Trseg: Transformer for semantic segmentation. *Pattern Recognit. Lett.*, 148:29–35, 2021. 3
- [44] Alexander Kirillov, Ross Girshick, Kaiming He, and Piotr Dollár. Panoptic feature pyramid networks. In *Proceedings of the IEEE/CVF Conference on Computer Vision and Pattern Recognition*, pages 6399–6408, 2019. 9
- [45] D. Kondratyuk, Liangzhe Yuan, Yandong Li, Li Zhang, Mingxing Tan, Matthew A. Brown, and Boqing Gong. Movinets: Mobile video networks for efficient video recognition. *ArXiv*, abs/2103.11511, 2021. 7, 8
- [46] Alex Krizhevsky, Ilya Sutskever, and Geoffrey E Hinton. Imagenet classification with deep convolutional neural networks. In F. Pereira, C. J. C. Burges, L. Bottou, and K. Q. Weinberger, editors, *Advances in Neural Information Processing Systems*, volume 25. Curran Associates, Inc., 2012. 3
- [47] Heeseung Kwon, Manjin Kim, Suha Kwak, and Minsu Cho. Motion-squeeze: Neural motion feature learning for video understanding. In *ECCV*, 2020. 8
- [48] Ke Li, Shijie Wang, Xiang Zhang, Yifan Xu, Weijian Xu, and Zhuowen Tu. Pose recognition with cascade transformers. *2021 IEEE/CVF Conference on Computer Vision and Pattern Recognition (CVPR)*, pages 1944–1953, 2021. 10
- [49] Kunchang Li, Xianhang Li, Yali Wang, Jun Wang, and Y. Qiao. Ct-net: Channel tensorization network for video classification. *ArXiv*, abs/2106.01603, 2021. 3, 8
- [50] X. Li, Yali Wang, Zhipeng Zhou, and Yu Qiao. Smallbignet: Integrating core and contextual views for video classification. *2020 IEEE Conference on Computer Vision and Pattern Recognition (CVPR)*, pages 1089–1098, 2020. 1, 3, 8
- [51] Yanjie Li, Shoukui Zhang, Zhicheng Wang, Sen Yang, Wankou Yang, Shutao Xia, and Erjin Zhou. Tokenpose: Learning keypoint tokens for human pose estimation. *ArXiv*, abs/2104.03516, 2021. 3, 10
- [52] Yinong Li, Bin Ji, Xintian Shi, Jianguo Zhang, Bin Kang, and Limin Wang. Tea: Temporal excitation and aggregation for action recognition. *ArXiv*, abs/2004.01398, 2020. 3, 8
- [53] Jingyun Liang, Jie Cao, Guolei Sun, K. Zhang, Luc Van Gool, and Radu Timofte. Swinir: Image restoration using swin transformer. *2021 IEEE/CVF International Conference on Computer Vision Workshops (ICCVW)*, pages 1833–1844, 2021. 3
- [54] Ji Lin, Chuang Gan, and Song Han. Tsm: Temporal shift module for efficient video understanding. *2019 IEEE International Conference on Computer Vision (ICCV)*, pages 7082–7092, 2019. 3, 8
- [55] Tsung-Yi Lin, Michael Maire, Serge Belongie, James Hays, Pietro Perona, Deva Ramanan, Piotr Dollár, and C Lawrence Zitnick. Microsoft coco: Common objects in context. In *European conference on computer vision*, pages 740–755. Springer, 2014. 3, 6, 8, 9
- [56] Ze Liu, Yutong Lin, Yue Cao, Han Hu, Yixuan Wei, Zheng Zhang, S. Lin, and B. Guo. Swin transformer: Hierarchical vision transformer using shifted windows. *ArXiv*, abs/2103.14030, 2021. 1, 3, 5, 6, 7, 8, 9, 10
- [57] Ze Liu, Jia Ning, Yue Cao, Yixuan Wei, Zheng Zhang, S. Lin, and Han Hu. Video swin transformer. *ArXiv*, abs/2106.13230, 2021. 1, 3, 8
- [58] Zhaoyang Liu, D. Luo, Yabiao Wang, L. Wang, Ying Tai, Chengjie Wang, Jilin Li, Feiyue Huang, and Tong Lu. Teinet: Towards an efficient architecture for video recognition. *ArXiv*, abs/1911.09435, 2020. 3, 8
- [59] Zhouyong Liu, Shun Luo, Wubin Li, Jingben Lu, Yufan Wu, Chunguo Li, and Luxi Yang. Convtransformer: A convolutional transformer network for video frame synthesis. *ArXiv*, abs/2011.10185, 2020. 3
- [60] I. Loshchilov and F. Hutter. Fixing weight decay regularization in adam. *ArXiv*, abs/1711.05101, 2017. 6, 7
- [61] Ilya Loshchilov and Frank Hutter. Sgdr: Stochastic gradient descent with warm restarts. *arXiv: Learning*, 2017. 6, 7, 9
- [62] Chenxu Luo and Alan L. Yuille. Grouped spatial-temporal aggregation for efficient action recognition. *2019 IEEE International Conference on Computer Vision (ICCV)*, pages 5511–5520, 2019. 3, 8
- [63] Daniel Neimark, Omri Bar, Maya Zohar, and Dotan Asselmann. Video transformer network. *ArXiv*, abs/2102.00719, 2021. 8
- [64] Mandela Patrick, Dylan Campbell, Yuki M. Asano, Ishan Misra Florian Metze, Christoph Feichtenhofer, A. Vedaldi, and João F. Henriques. Keeping your eye on the ball: Trajectory attention in video transformers. *ArXiv*, abs/2106.05392, 2021. 3, 8
- [65] Zhaofan Qiu, Ting Yao, and Tao Mei. Learning spatio-temporal representation with pseudo-3d residual networks. *2017 IEEE International Conference on Computer Vision (ICCV)*, pages 5534–5542, 2017. 3
- [66] Zhaofan Qiu, Ting Yao, C. Ngo, Xinmei Tian, and Tao Mei. Learning spatio-temporal representation with local and global diffusion. *2019 IEEE/CVF Conference on Computer Vision and Pattern Recognition (CVPR)*, pages 12048–12057, 2019. 8
- [67] Ilija Radosavovic, Raj Prateek Kosaraju, Ross B. Girshick, Kaiming He, and Piotr Dollár. Designing network design spaces. *2020 IEEE/CVF*

- Conference on Computer Vision and Pattern Recognition (CVPR)*, pages 10425–10433, 2020. 7
- [68] Prajit Ramachandran, Niki Parmar, Ashish Vaswani, Irwan Bello, Anselm Levskaya, and Jonathon Shlens. Stand-alone self-attention in vision models. In *NeurIPS*, 2019. 3, 6
- [69] Mark Sandler, Andrew Howard, Menglong Zhu, Andrey Zhmoginov, and Liang-Chieh Chen. Mobilenetv2: Inverted residuals and linear bottlenecks. In *Proceedings of the IEEE conference on computer vision and pattern recognition*, pages 4510–4520, 2018. 3, 4, 10
- [70] Ramprasaath R. Selvaraju, Abhishek Das, Ramakrishna Vedantam, Michael Cogswell, Devi Parikh, and Dhruv Batra. Grad-cam: Visual explanations from deep networks via gradient-based localization. *International Journal of Computer Vision*, 128:336–359, 2019. 12
- [71] Gilad Sharir, Asaf Noy, and Lih Zelnik-Manor. An image is worth 16x16 words, what is a video worth? *ArXiv*, abs/2103.13915, 2021. 4, 8
- [72] Karen Simonyan and Andrew Zisserman. Very deep convolutional networks for large-scale image recognition. *arXiv preprint arXiv:1409.1556*, 2014. 3
- [73] A. Srinivas, Tsung-Yi Lin, Niki Parmar, Jonathon Shlens, P. Abbeel, and Ashish Vaswani. Bottleneck transformers for visual recognition. *ArXiv*, abs/2101.11605, 2021. 7
- [74] Chen Sun, Abhinav Shrivastava, Saurabh Singh, and Abhinav Kumar Gupta. Revisiting unreasonable effectiveness of data in deep learning era. *2017 IEEE International Conference on Computer Vision (ICCV)*, pages 843–852, 2017. 8
- [75] Christian Szegedy, Wei Liu, Yangqing Jia, Pierre Sermanet, Scott E. Reed, Dragomir Anguelov, D. Erhan, Vincent Vanhoucke, and Andrew Rabinovich. Going deeper with convolutions. *2015 IEEE Conference on Computer Vision and Pattern Recognition (CVPR)*, pages 1–9, 2015. 3
- [76] Mingxing Tan and Quoc V. Le. Efficientnet: Rethinking model scaling for convolutional neural networks. *ArXiv*, abs/1905.11946, 2019. 3, 7
- [77] Mingxing Tan and Quoc V. Le. Efficientnetv2: Smaller models and faster training. *ArXiv*, abs/2104.00298, 2021. 7
- [78] Hugo Touvron, M. Cord, M. Douze, Francisco Massa, Alexandre Sablayrolles, and Hervé Jégou. Training data-efficient image transformers & distillation through attention. In *ICML*, 2021. 1, 2, 3, 5, 6, 7, 9
- [79] Hugo Touvron, M. Cord, Alexandre Sablayrolles, Gabriel Synnaeve, and Hervé Jégou. Going deeper with image transformers. *ArXiv*, abs/2103.17239, 2021. 1, 5, 6, 7
- [80] Du Tran, Lubomir D. Bourdev, Rob Fergus, Lorenzo Torresani, and Manohar Paluri. Learning spatiotemporal features with 3d convolutional networks. *2015 IEEE International Conference on Computer Vision (ICCV)*, pages 4489–4497, 2015. 3
- [81] Du Tran, Heng Wang, L. Torresani, and Matt Feiszli. Video classification with channel-separated convolutional networks. *2019 IEEE/CVF International Conference on Computer Vision (ICCV)*, pages 5551–5560, 2019. 3, 4, 8, 10
- [82] Du Tran, Hong xiu Wang, Lorenzo Torresani, Jamie Ray, Yann LeCun, and Manohar Paluri. A closer look at spatiotemporal convolutions for action recognition. *2018 IEEE Conference on Computer Vision and Pattern Recognition (CVPR)*, pages 6450–6459, 2018. 3
- [83] Ashish Vaswani, Noam M. Shazeer, Niki Parmar, Jakob Uszkoreit, Llion Jones, Aidan N. Gomez, Lukasz Kaiser, and Illia Polosukhin. Attention is all you need. *ArXiv*, abs/1706.03762, 2017. 5
- [84] Heng Wang, Du Tran, L. Torresani, and Matt Feiszli. Video modeling with correlation networks. *2020 IEEE/CVF Conference on Computer Vision and Pattern Recognition (CVPR)*, pages 349–358, 2020. 8
- [85] Jingdong Wang, Ke Sun, Tianheng Cheng, Borui Jiang, Chaorui Deng, Yang Zhao, D. Liu, Yadong Mu, Mingkui Tan, Xinggang Wang, Wenyu Liu, and Bin Xiao. Deep high-resolution representation learning for visual recognition. *IEEE Transactions on Pattern Analysis and Machine Intelligence*, 43:3349–3364, 2021. 10
- [86] L. Wang, Yuanjun Xiong, Zhe Wang, Y. Qiao, D. Lin, X. Tang, and L. Gool. Temporal segment networks: Towards good practices for deep action recognition. In *ECCV*, 2016. 7, 8
- [87] Limin Wang, Zhan Tong, Bin Ji, and Gangshan Wu. Tdn: Temporal difference networks for efficient action recognition. *ArXiv*, abs/2012.10071, 2020. 8
- [88] Ning Wang, Wen gang Zhou, Jie Wang, and Houqiang Li. Transformer meets tracker: Exploiting temporal context for robust visual tracking. *2021 IEEE/CVF Conference on Computer Vision and Pattern Recognition (CVPR)*, pages 1571–1580, 2021. 3
- [89] Wenhai Wang, Enze Xie, Xiang Li, Deng-Ping Fan, Kaitao Song, Ding Liang, Tong Lu, P. Luo, and L. Shao. Pyramid vision transformer: A versatile backbone for dense prediction without convolutions. *ArXiv*, abs/2102.12122, 2021. 3, 5, 7, 9
- [90] X. Wang, Ross B. Girshick, Abhinav Gupta, and Kaiming He. Non-local neural networks. *2018 IEEE/CVF Conference on Computer Vision and Pattern Recognition*, pages 7794–7803, 2018. 1, 3, 7, 11
- [91] Haiping Wu, Bin Xiao, N. Codella, Mengchen Liu, Xiyang Dai, Lu Yuan, and Lei Zhang. Cvt: Introducing convolutions to vision transformers. *ArXiv*, abs/2103.15808, 2021. 3, 7
- [92] Bin Xiao, Haiping Wu, and Yichen Wei. Simple baselines for human pose estimation and tracking. In *ECCV*, 2018. 10
- [93] Tete Xiao, Yingcheng Liu, Bolei Zhou, Yuning Jiang, and Jian Sun. Unified perceptual parsing for scene understanding. In *Proceedings of the European Conference on Computer Vision (ECCV)*, pages 418–434, 2018. 9
- [94] Tete Xiao, Mannat Singh, Eric Mintun, Trevor Darrell, Piotr Dollár, and Ross B. Girshick. Early convolutions help transformers see better. *ArXiv*, abs/2106.14881, 2021. 3
- [95] Enze Xie, Wenhai Wang, Zhiding Yu, Anima Anandkumar, Jose M Alvarez, and Ping Luo. Segformer: Simple and efficient design for semantic segmentation with transformers. *arXiv preprint arXiv:2105.15203*, 2021. 3
- [96] Saining Xie, Ross B. Girshick, Piotr Dollár, Zhuowen Tu, and Kaiming He. Aggregated residual transformations for deep neural networks. *2017 IEEE Conference on Computer Vision and Pattern Recognition (CVPR)*, pages 5987–5995, 2017. 1, 3, 9
- [97] Jianwei Yang, Chunyuan Li, Pengchuan Zhang, Xiyang Dai, Bin Xiao, Lu Yuan, and Jianfeng Gao. Focal self-attention for local-global interactions in vision transformers. *arXiv preprint arXiv:2107.00641*, 2021. 3, 6, 7, 9, 10
- [98] Sen Yang, Zhibin Quan, Mu Nie, and Wankou Yang. Transpose: Towards explainable human pose estimation by transformer. *ArXiv*, abs/2012.14214, 2020. 3, 10
- [99] Kun Yuan, Shaopeng Guo, Ziwei Liu, Aojun Zhou, Fengwei Yu, and Wei Wu. Incorporating convolution designs into visual transformers. *ArXiv*, abs/2103.11816, 2021. 3
- [100] Li Yuan, Y. Chen, Tao Wang, Weihao Yu, Yujun Shi, Francis E. H. Tay, Jiashi Feng, and Shuicheng Yan. Tokens-to-token vit: Training vision transformers from scratch on imagenet. *ArXiv*, abs/2101.11986, 2021. 7
- [101] Li Yuan, Qibin Hou, Zihang Jiang, Jiashi Feng, and Shuicheng Yan. Volo: Vision outlooker for visual recognition. *ArXiv*, abs/2106.13112, 2021. 7
- [102] Yuhui Yuan, Rao Fu, Lang Huang, Weihong Lin, Chao Zhang, Xilin Chen, and Jingdong Wang. Hrformer: High-resolution transformer for dense prediction. *ArXiv*, abs/2110.09408, 2021. 3, 10
- [103] Sangdoon Yun, Dongyoon Han, Seong Joon Oh, Sanghyuk Chun, Junsuk Choe, and Young Joon Yoo. Cutmix: Regularization strategy to train strong classifiers with localizable features. *2019 IEEE/CVF International Conference on Computer Vision (ICCV)*, pages 6022–6031, 2019. 6
- [104] David Junhao Zhang, Kunchang Li, Yunpeng Chen, Yali Wang, Shashwat Chandra, Yu Qiao, Luoqi Liu, and Mike Zheng Shou. Morphmlp: A self-attention free, mlp-like backbone for image and video. *arXiv preprint arXiv:2111.12527*, 2021. 1
- [105] Hang Zhang, Chongruo Wu, Zhongyue Zhang, Yi Zhu, Haibin Lin, Zhi Zhang, Yue Sun, Tong He, Jonas Mueller, R Manmatha, et al. Resnest: Split-attention networks. *arXiv preprint arXiv:2004.08955*, 2020. 1
- [106] Hongyi Zhang, Moustapha Cissé, Yann Dauphin, and David Lopez-Paz. mixup: Beyond empirical risk minimization. *ArXiv*, abs/1710.09412, 2018. 6
- [107] Pengchuan Zhang, Xiyang Dai, Jianwei Yang, Bin Xiao, Lu Yuan, Lei Zhang, and Jianfeng Gao. Multi-scale vision longformer: A new vision transformer for high-resolution image encoding. *ArXiv*, abs/2103.15358, 2021. 9
- [108] Xiangyu Zhang, Xinyu Zhou, Mengxiao Lin, and Jian Sun. Shufflenet: An extremely efficient convolutional neural network for mobile devices. *2018 IEEE/CVF Conference on Computer Vision and Pattern Recognition*, pages 6848–6856, 2018. 3
- [109] Bolei Zhou, Hang Zhao, Xavier Puig, Tete Xiao, Sanja Fidler, Adela Barriuso, and Antonio Torralba. Semantic understanding of scenes through the ade20k dataset. *International Journal of Computer Vision*, 127(3):302–321, 2019. 3, 6, 9
- [110] Hong-Yu Zhou, Chixiang Lu, Sibe Yang, and Yizhou Yu. Convnets vs. transformers: Whose visual representations are more transferable? *ArXiv*, abs/2108.05305, 2021. 8
- [111] Xizhou Zhu, Weijie Su, Lewei Lu, Bin Li, Xiaogang Wang, and Jifeng Dai. Deformable detr: Deformable transformers for end-to-end object detection. *ArXiv*, abs/2010.04159, 2021. 3